

## Multiple-Stage Structure Transformation of Organic-Inorganic Hybrid Perovskite $\text{CH}_3\text{NH}_3\text{PbI}_3$

Qiong Chen,<sup>1</sup> Henan Liu,<sup>2</sup> Hui-Seon Kim,<sup>3</sup> Yucheng Liu,<sup>4</sup> Mengjin Yang,<sup>5</sup> Naili Yue,<sup>6</sup> Gang Ren,<sup>6</sup>  
Kai Zhu,<sup>5</sup> Shengzhong Liu,<sup>4</sup> Nam-Gyu Park,<sup>3</sup> and Yong Zhang<sup>1,2,\*</sup>

<sup>1</sup>*Department of Electrical and Computer Engineering, The University of North Carolina at Charlotte, Charlotte, North Carolina 28223, USA*

<sup>2</sup>*Graduate Programs in Optical Science and Engineering, The University of North Carolina at Charlotte, Charlotte, North Carolina 28223, USA*

<sup>3</sup>*School of Chemical Engineering and Department of Energy Science, Sungkyunkwan University, Suwon 440-746, South Korea*

<sup>4</sup>*Key Laboratory of Applied Surface and Colloid Chemistry, National Ministry of Education; Institute for Advanced Energy Materials, School of Materials Science and Engineering, Shaanxi Normal University, Xi'an 710062, China*

<sup>5</sup>*Chemical and Materials Science Center, National Renewable Energy Laboratory, Golden, Colorado 80401, USA*

<sup>6</sup>*Molecular Foundry, Lawrence Berkeley National Laboratory, Berkeley, California 94720, USA*

(Received 16 April 2016; published 15 September 2016)

By performing spatially resolved Raman and photoluminescence spectroscopy with varying excitation wavelength, density, and data acquisition parameters, we achieve a unified understanding towards the spectroscopy signatures of the organic-inorganic hybrid perovskite, transforming from the pristine state ( $\text{CH}_3\text{NH}_3\text{PbI}_3$ ) to the fully degraded state (i.e.,  $\text{PbI}_2$ ) for samples with varying crystalline domain size from mesoscopic scale (approximately 100 nm) to macroscopic size (centimeters), synthesized by three different techniques. We show that the hybrid perovskite exhibits multiple stages of structure transformation occurring either spontaneously or under light illumination, with exceptionally high sensitivity to the illumination conditions (e.g., power, illumination time, and interruption pattern). We highlight four transformation stages (stages I–IV, with stage I being the pristine state) along either the spontaneous or photoinduced degradation path exhibiting distinctly different Raman spectroscopy features at each stage, and point out that previously reported Raman spectra in the literature reflect highly degraded structures of either stage III or stage IV. Additional characteristic optical features of partially degraded materials under the joint action of spontaneous and photodegradation are also given. This study offers reliable benchmark results for understanding the intrinsic material properties and structure transformation of this unique category of hybrid materials, and the findings are pertinently important to a wide range of potential applications where the hybrid material is expected to function in greatly different environment and light-matter interaction conditions.

DOI: [10.1103/PhysRevX.6.031042](https://doi.org/10.1103/PhysRevX.6.031042)

Subject Areas: Energy Research, Materials Science

### I. INTRODUCTION

As a solar-cell absorber material, organic-inorganic hybrid structure ( $\text{CH}_3\text{NH}_3$ ) $\text{PbI}_3$  (MAPbI<sub>3</sub>) is perhaps the material that has shown the fastest efficiency growth among all the currently known absorber materials [1–7]. While in its first use in a sensitized solar cell in 2009 it had a reported efficiency of 3.8% [1], today the reported efficiency has exceeded 20%, an important milestone shared by only two other thin-film solar-cell technologies based on CdTe and

CIGS. However, this material system is facing a critical challenge, that is, structural stability [8]. The rapid progress in the device performance has led to explosive research activities on the material properties, in particular, optical properties [9]. Unfortunately, some optical characterization work has been done in a rush without paying sufficient attention to the extreme structural instability, thus yielding results extrinsic to the material. Roughly speaking, if the photodegradation threshold of an ionic compound like  $\text{Cu}_2\text{ZnSnSe}_4$  is 2 orders of magnitude lower than covalent or mostly covalent semiconductors like Si and GaAs [10,11], MAPbI<sub>3</sub> is further lower by 2 orders more, as we demonstrate in this work. Therefore, extra caution is required in optical characterization. The primary intent of this work is to reveal the intrinsic optical properties and signatures of different stages of natural degradation and

\*yong.zhang@uncc.edu

Published by the American Physical Society under the terms of the *Creative Commons Attribution 3.0 License*. Further distribution of this work must maintain attribution to the author(s) and the published article's title, journal citation, and DOI.

photodegradation, and, thus, provide reliable information for further investigation of the material. Furthermore, the derived information provides guidance to different anticipated applications, from solar cell, sensor, and laser, to photonic structure, where the hybrid material is expected to operate in vastly different environment and light-matter interaction conditions.

Organic-inorganic hybrid materials tend to appear in disordered phases [12]. There are only very limited examples of truly ordered hybrid materials that can be considered as crystals in a genuine sense, i.e., having a translational symmetry. Only in a few rare cases can the very high degree structural ordering yield x-ray diffraction peaks and Raman lines as sharp as a high-quality semiconductor like GaAs, as in some hybrid structures based on II-VI semiconductors, such as  $\text{ZnTe}(\text{en})_{0.5}$ , where  $\text{en} = \text{C}_2\text{N}_2\text{H}_8$  [13,14]. One key factor to have a highly ordered hybrid structure is understandably to involve only small organic molecules. The hybrid perovskite structure  $\text{MAPbI}_3$  would seem to be a good candidate applying this simple intuition. However, because of the orientational disorder of the molecular cation  $\text{MA}^+$ , the structure is, strictly speaking, disordered (dynamic disorder) [15]. Although  $\text{MAPbI}_3$  is often referred to as having a tetragonal symmetry in the temperature region of approximately 162–327 K (cubic at higher and orthorhombic at lower temperature regions, respectively) [15], the symmetry should be understood in the same sense as in the case of a semiconductor alloy to be an averaged symmetry. While it is well known that the alloying effect leads to linewidth broadening in many spectroscopy features in semiconductor alloys [16], the disordering effect is expected to manifest in the perovskite hybrid in a similar manner.

Raman spectroscopy is an effective tool for probing the disordering effect as well as the disorder-order transition in semiconductors [17,18]. The inorganic counterpart of  $\text{MAPbCl}_3$ ,  $\text{CsPbCl}_3$ , is known to be Raman inactive in first-order scattering when in the cubic phase [19,20], as is true for the cubic  $\text{SrTiO}_3$  [21,22]. However, tetragonal and orthorhombic  $\text{CsPbCl}_3$  become Raman active [19,20]. A subtle but important difference is expected between the inorganic and hybrid perovskite. The disorder will relax the Raman selection for the cubic phase, i.e., the first-order Raman will become partially allowed, but in the meantime results in spectral broadening, which will manifest as a disorder activated band reflecting the phonon density of states, as was observed in a similar system  $\text{MAPbCl}_3$  for its room-temperature cubic phase [23]. Even for its tetragonal phase, some phonon modes are, in principle, Raman allowed, but the disordering effect still dominates over the symmetry dictated effect; i.e., no distinct Raman mode is actually observed. Only for the low-temperature orthorhombic phase were many distinct Raman peaks observed, indicating that the structure became highly ordered [23]. Since  $\text{MAPbI}_3$  is in tetragonal phase at room temperature,

and likely more disordered than tetragonal  $\text{MAPbCl}_3$  due to the larger void for the molecule and higher temperature, the finding for  $\text{MAPbCl}_3$  might hint that no distinct Raman mode should be observed for  $\text{MAPbI}_3$  at room temperature. The situation in  $\text{MAPbI}_3$  is further more complicated than in  $\text{MAPbCl}_3$ , because of the lower environmental and photostability of the former, which seems to be related to the larger anion for the former. It was found similarly for the II-VI-based hybrids [13] that the photostability reduced with increasing anion size in common cation isostructures [e.g.,  $\text{CdX}(\text{ba})_{0.5}$ , where  $X = \text{S}, \text{Se}, \text{and Te}$ ]. Another subtle effect could be significant, that is, the dependence on the domain size in  $\text{MAPbI}_3$  polycrystalline films. Even in an ordered inorganic semiconductor alloy,  $\text{In}_{0.5}\text{Ga}_{0.5}\text{P}$ , for example, its small domain size makes it much more challenging to observe ordering-induced Raman features [24]. Given the fact that the hybrid perovskite materials have been synthesized using a wide range of techniques [3–6,25,26], resulting in vast differences in crystalline domain size, interface, and surface, it is of great interest to ask if these different structures share common vibrational signatures that are intrinsic to the hybrid structure of interest.

The reported Raman spectroscopy results for  $\text{MaPbI}_3$  have, in fact, shown great diversity. The room-temperature Raman data can be grouped into two categories: type 1, with relatively weak and broad bands at 52–69, 94, 108–119  $\text{cm}^{-1}$  [27–30], and type 2, with stronger and well-resolved peaks at 71, 94–95, 110–111  $\text{cm}^{-1}$  [31,32]. Type 2 in fact closely resembles 2H-PbI<sub>2</sub> Raman modes at 74 ( $E_g$ ), 96 ( $A_{1g}$ ), and 110 or 106/113  $\text{cm}^{-1}$  ( $A_{2u}/2E_u$ ) [33–37]. A transition from type 1 to type 2 was observed with either increasing excitation power or prolonged illumination [29–31]. The transition was explained as photodegradation from  $\text{MAPbI}_3$  to  $\text{PbI}_2$  [29], but was indicated to be reversible and attributed to the photo-induced structural transformation of perovskite [30]. It is apparently unclear which set, if any, of these Raman features is intrinsic to  $\text{MAPbI}_3$  or if they represent two structural variations of the perovskite framework. Note that these studies were performed using samples prepared by various techniques with one obvious variation, the polycrystalline domain size. Furthermore, the small variation in experimental conditions, such as the illumination power density and data acquisition time, could mean that the photoinduced transition is reversible or irreversible, keeping in mind that the measurements were often performed using micro-Raman systems usually involving high excitation density and the structural transformation often is an exponential activation process of the external perturbation. In our recent study using a moderately high excitation density, the hybrid perovskite Raman spectrum has been found to be domain size dependent, with that of the small domain resembling type 2, whereas that of the large domain resembles the mixture of the two sets but both being well resolved [38]. Therefore, there is apparently considerable

inconsistency, ambiguity, and uncertainty between the reported data and regarding which represents the intrinsic properties of the material.

In this work, we attempt to address the following questions. (1) Are the above-mentioned observations all intrinsic to the hybrid perovskite? (2) If yes, what are the likely underlying mechanisms for the variations? (3) If no, what should be the intrinsic spectroscopic features? To this end, we perform spatially resolved Raman-PL studies on a set of samples including polycrystalline films of different domain sizes and sources as well as single crystals, with varying excitation wavelength, density, and acquisition parameters. The direct comparison of the results from the same measurement system removes the possible uncertainty when comparing data from different publications, and, thus, is able to offer a unified understanding for the materials with distinctly different preparation methods and crystalline domain structures.

## II. EXPERIMENT

MAPbI<sub>3</sub> samples from three sources are used in this work: (1) polycrystalline films synthesized by the Sungkyunkwan University (SKKU) group that consist of polycrystalline domains typically  $\sim 500$  nm in size (referred to as SKKU-p), and isolated larger domains of

$\sim 5\text{--}10$   $\mu\text{m}$  found on the film (referred to as SKKU-L) [38,39], (2) small domain polycrystalline films by the National Renewable Energy Laboratory (NREL) group (NREL-p) [40], and (3) macroscopic size (millimeters to centimeters) single crystalline samples by the Shaanxi Normal University (SNU) group (SNU-c) [26]. There are effectively four distinctly different types of samples. Samples were received vacuum packed, and kept in a continuously pumped chamber, to prolong the sample lifetime (typically up to a few months). Both the SKKU and NREL samples are deposited on glass with a TiO<sub>2</sub> buffer layer [39,40], whereas the SMU samples are freestanding crystals [26]. None of them have any top protection layer. Figure 1 provides the basic structural information of the samples. Figures 1(a) and 1(b) show the typical SEM images for the morphology information of the as-grown SKKU and NREL samples, respectively, and Fig. 1(c) is a SEM image of a degraded SKKU sample that has been left under ambient condition for a few weeks and fully converted back into PbI<sub>2</sub>. Figure 1(d) is a SEM image of SNU-c sample of a large single crystal, showing uniform surface.

The optical properties of the hybrid perovskite are very sensitive to the measurement conditions, particularly excitation wavelength  $\lambda$ , excitation power  $P$ , or more relevant

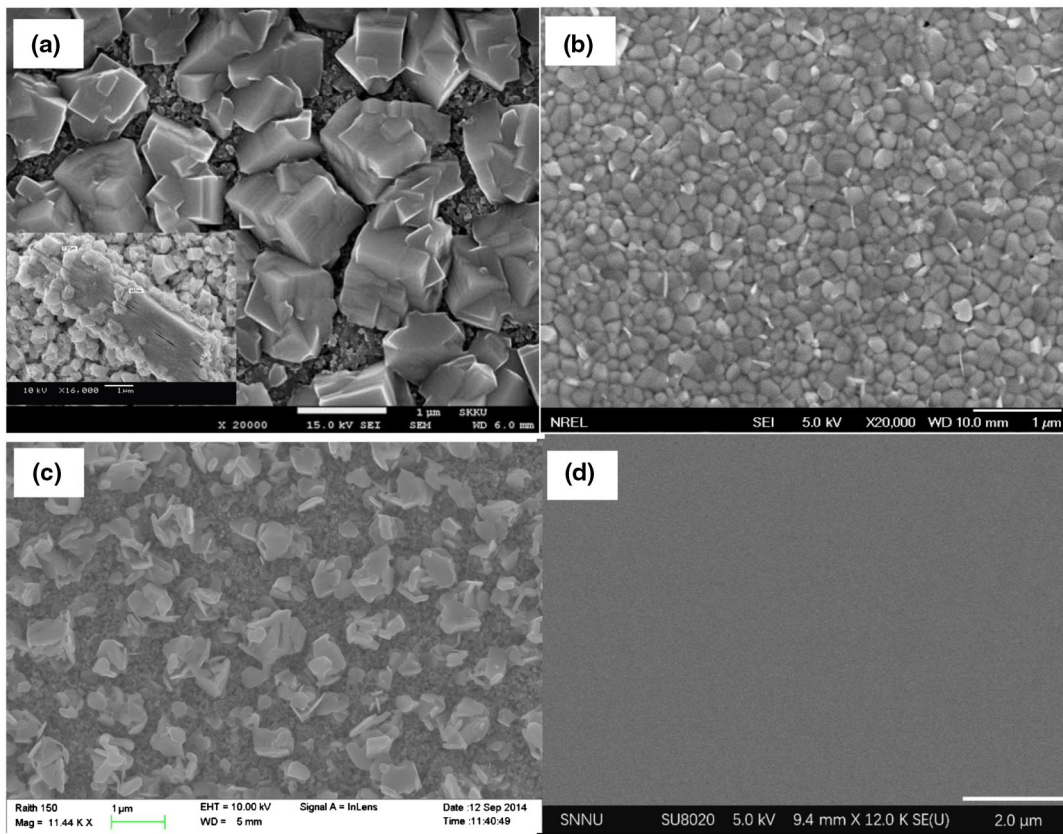


FIG. 1. SEM images of MAPbI<sub>3</sub> hybrid perovskite samples: (a) a SKKU-p sample (with a large domain shown as an inset), (b) a NREL-p sample, (c) a degraded SKKU-p sample, (d) a SNU-c sample.

density  $D$ , which in turn depend on the wavelength and numerical aperture (NA) of the microscope lens and data collection time. Previously used power densities range from about 1 to 16 kW/cm<sup>2</sup> on the lower end [29,30] to 86–110 kW/cm<sup>2</sup> on the higher end [31,32]. In this work, we use excitation densities varying from about 170 W to 50 kW/cm<sup>2</sup>, allowing more careful examination of the possible heating and photodegradation effects. Often not specifically mentioned in the literature (except for Ref. [30]), the acquisition time is a significant parameter in addition to the excitation density. In this work, we also examine the effects of total acquisition time (TAT, the actual data acquisition time excluding interruption time) as well as interruption time (IT) between continued data collection time (CT). Data are taken using either a 100 $\times$  (NA = 0.9) or a 50  $\times$  L (NA = 0.5, long working distance) microscope lens on a Horiba LabRam HR800 confocal Raman microscope with a 1200 g/mm grating, using a 532- and 441.6-nm laser with a full power of  $\sim$ 18 and  $\sim$ 13 mW, respectively, measured when exiting the microscope lens. The excitation density is estimated as  $D = P/A$ , where  $A$  is the area determined by the diffraction limit spot size  $1.22\lambda/NA$ . The laser power is attenuated either using built-in attenuators D1–D4, from high to low, approximately giving 1–4 order attenuation, or by reducing the operation current of the laser. At D4, for the 532- (442-) nm laser, the excitation densities are approximately 440 (460) or 136(142) W/cm<sup>2</sup>, respectively, with a 100 $\times$  or 50  $\times$  L lens. The lowest excitation density used is significantly lower than the lowest level used in the previous reports, and is considered very low for the confocal measurement and comparable to that in a typical macroscopic measurement, although still much higher than solar radiation (0.1 W/cm<sup>2</sup> for AM1.5). In comparison to other Photovoltaic (PV) materials like Si that will not show any photodegradation under  $> 10^6$  W/cm<sup>2</sup> excitation, the hybrid has very low photostability because prolonged illumination can lead to structural transformation even with 100 W/cm<sup>2</sup> level illumination. To minimize or examine heating and/or photodegradation effects, a mechanical shutter is employed to block the laser beam in a Raman measurement (1) when the CCD detector is not actively taking data and (2) periodically during a long data collection cycle. The measurements are performed at room temperature with continued low N<sub>2</sub> flow over the sample surface to slow down the sample degradation when exposed to ambient condition (no significant change for a few hours).

### III. RESULTS AND DISCUSSIONS

#### A. Intrinsic optical properties probed by Raman and photoluminescence

We first attempt to address the question of what to expect in the Raman spectrum of a pristine hybrid perovskite MAPbI<sub>3</sub>. It turns out that all the Raman spectra reported in

the literature show the spectroscopic signatures of some degree of spontaneous and/or photoinduced structure degradation, based on our analyses of four representative types of samples we describe herein.

#### 1. SKKU-p samples

Figure 2 compares Raman and photoluminescence spectra of a few SKKU samples that were measured at different delay times after the samples were received, reflecting different degrees in natural degradation. Figures 2(a) and 2(b) include five representative Raman spectra from five samples using the 532-nm laser, where SKKU-p-1 to SKKU-p-4 are measured on a single spatial spot under D/TAT/CT/IT = D4<sub>100 $\times$</sub> /800 s/0.5 s/0.5 s (except for SKKU-p-3 under D4<sub>50 $\times$ L</sub>), and SKKU-p-5 is measured under the same excitation level of SKKU-p-1 but only for 1 s per spatial point and averaging over 2420 total spatial points in an interval of 5  $\mu$ m (D/TAT/CT = D4<sub>100 $\times$</sub> /1 s/1 s). The SKKU-p-5 measurement is to minimize any potential accumulative effect of the large total illumination time in the other cases. These samples represent different stages of spontaneous or natural degradation, corresponding to different lengths in the exposure time to air. The degradation is manifested in the evolution of two major spectral features: (1) in the vicinity of 100 cm<sup>-1</sup>, from no visible feature above a smooth background in SKKU-p-1, to the emergence of a small “bump” in SKKU-p-2, to two resolvable peaks in SKKU-p-3, and finally to multiple well-developed sharp peaks in SKKU-p-4 that have almost fully converted back to PbI<sub>2</sub>; (2) a broad band  $\sim$ 550 cm<sup>-1</sup> with a valley at  $\sim$ 900 cm<sup>-1</sup> exhibits a systematic intensity reduction till it completely vanishes from SKKU-p-1 to SKKU-p-4. This broad band was absent in the previous reports and is confirmed to be Raman signal, because very similar spectra were obtained with 442-nm excitation (spectra not shown). The result of the additional sample SKKU-p-5 confirms that the spectrum of SKKU-p-1 can indeed represent that of a pristine sample. Clearly, the spectra of SKKU-p-1 and SKKU-p-5 are the two closest to each other. The comparison between SKKU-p-1 and SKKU-p-4 indicates that the Raman cross sections near 100 cm<sup>-1</sup> are at least a factor of 15 difference between PbI<sub>2</sub> and MAPbI<sub>3</sub>. Figure 2(c) compares the PL spectra of the same samples measured from the same spot as that for the respective Raman spectrum (taken before the Raman measurement) using the 442-nm laser under D4<sub>100 $\times$</sub> /1 s/1 s (D4<sub>50 $\times$ L</sub>/1 s/1 s for SKKU-p-3) in order to examine the PL emission not only near the band gap of the hybrid but also that of PbI<sub>2</sub>. We notice that with increasing level of degradation, the hybrid-related PL peak exhibits major peak intensity reduction, for over 4 orders in magnitude from SKKU-p-1 to SKKU-p-4, accompanied by a blueshift in peak position, from  $\sim$ 769 nm in SKKU-p-1, which is near the hybrid band gap, [41,42], to  $\sim$ 743 nm in SKKU-p-4 (only visible under 532-nm excitation).

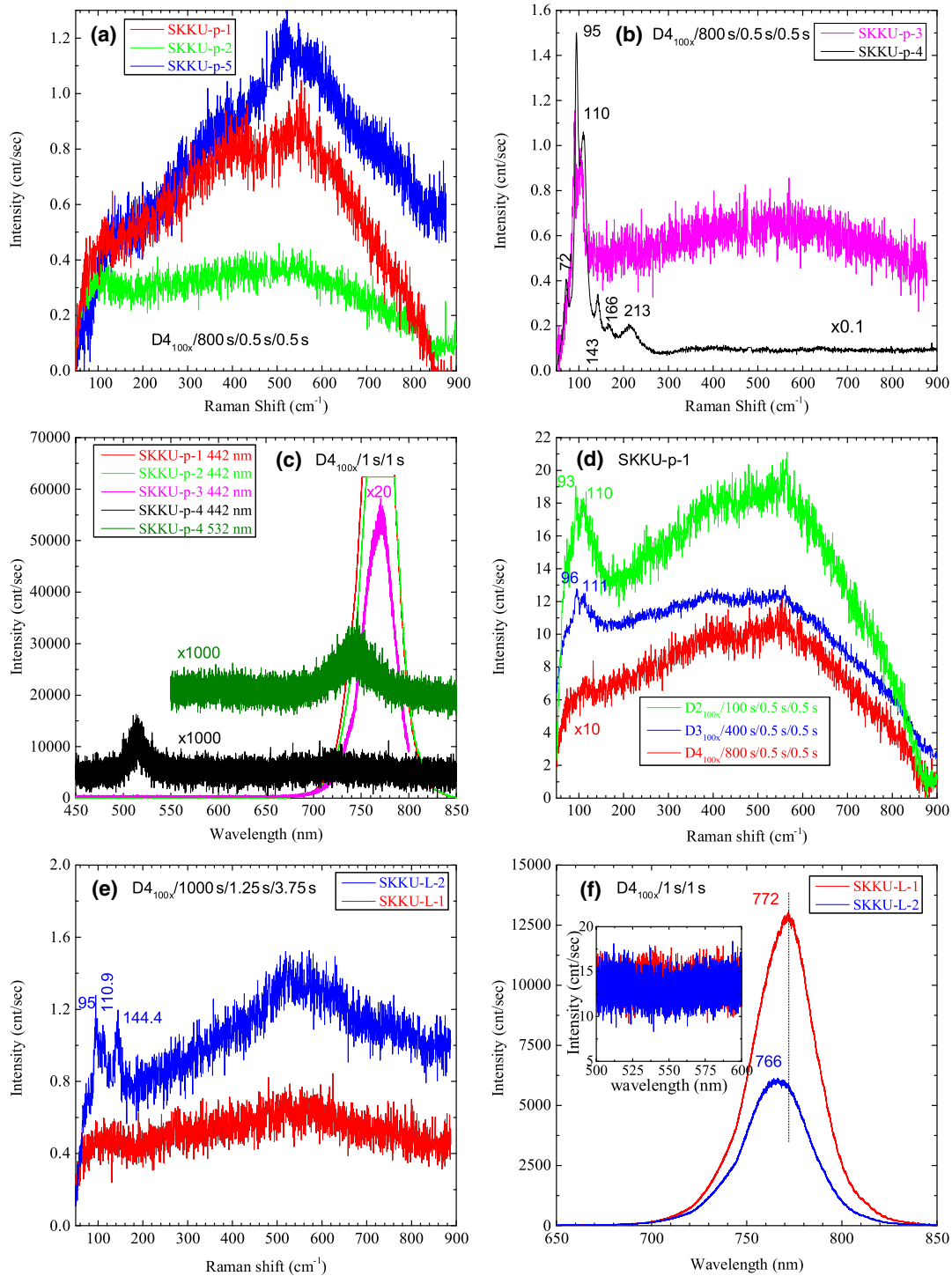


FIG. 2. Raman and PL spectra of SKKU samples at different stages of structure transformation. (a),(b) Representative Raman spectra at different stages of structure transformation from  $\text{MaPbI}_3$  to  $\text{PbI}_2$ , measured under a very low excitation density  $D4$  (SKKU-p-3 was measured with the  $50\times$  L lens, but multiplied by the laser density ratio between the  $100\times$  and  $50\times$  L lens). (c) PL spectra measured at  $D4$  from the same location as in (a) and (b) before the Raman measurement. (d) Raman excitation density dependence of the most pristine sample SKKU-p-1. (e) Low-excitation density ( $D4$ ) Raman spectra for two large-domain SKKU-L samples. (f) The corresponding PL spectra of (e), measured under  $D4$  before the Raman measurement. The inset shows the spectral region near the  $\text{PbI}_2$  band gap.

Additionally, in the most degraded sample, SKKU-p-4, a weak PL peak at  $\sim 514$  nm, which is close to the band gap of  $\text{PbI}_2$  [43] appears, whereas in the other samples this emission is invisible. The Raman spectrum of SKKU-p-4, despite being taken at a much lower excitation density level, resembles the type 2 spectrum for the hybrid material reported in the literature [31,32], but is also nearly the same as those reported for  $\text{PbI}_2$  [34,35]. The above results suggest that the Raman spectrum of SKKU-p-1 or SKKU-p-5 can be taken as that of a pristine  $\text{MAPbI}_3$ : no visible peak near  $100\text{ cm}^{-1}$  but with a broad band at  $\sim 550\text{ cm}^{-1}$ .

Figure 2(d) compares Raman spectra of the most pristine sample SKKU-p-1 measured under three conditions consecutively:  $\text{D}_{4_{100\times}}/800\text{ s}/0.5\text{ s}/0.5\text{ s}$ ,  $\text{D}_{3_{100\times}}/400\text{ s}/0.5\text{ s}/0.5\text{ s}$ , and  $\text{D}_{2_{100\times}}/100\text{ s}/0.5\text{ s}/0.5\text{ s}$ . For this type of sample, the combination of  $\text{D}_{4_{100\times}}/800\text{ s}/0.5\text{ s}/0.5\text{ s}$  appears to be a safe condition that does not result in a visible change in the overall shape of the Raman spectrum, although there may be some intensity reduction of the  $550\text{-cm}^{-1}$  peak. Under the other two conditions, two peaks are resolved at  $\sim 96$  and  $\sim 111$  or  $\sim 93$  and  $\sim 110\text{ cm}^{-1}$ , which are in fact similar to the type 1 spectra in the previous reports [27–30]. We note that in the Raman spectrum, despite the change near  $100\text{ cm}^{-1}$ , the  $\sim 550\text{-cm}^{-1}$  band remains after the two higher-level measurements; also in the PL spectrum (not shown), the hybrid band gap emission remains, and no emission near the  $\text{PbI}_2$  band gap is observed. This situation represents a subtle structural change of the hybrid without significant conversion back to  $\text{PbI}_2$ .

In our preliminary study using the  $\text{D}_{2_{50\times\text{L}}}$  excitation [38], the isolated large domains are found to yield much stronger signal and also exhibit more Raman features than the small ones, which now appears to be extrinsic in nature. Upon more careful and thorough examination, we suggest that the larger domains often contain incompletely reacted  $\text{PbI}_2$ , based on their Raman spectra and colors. Figure 2(e) compares the low-excitation density ( $\text{D}_{4_{100\times}}/1000\text{ s}/1.25\text{ s}/3.75\text{ s}$ ) Raman spectra of two large domains, SKKU-L-1 and SKKU-L-2, of which the former look similar in color to the regular sample area, but the latter appear brighter. The overall intensities are comparable to the small domain area (e.g., SKKU-p-1), but the brighter one exhibits  $\text{PbI}_2$ -like modes (similar to SKKU-p-4) superimposed on the intrinsic hybrid Raman spectrum. The difference could be explained as that the SKKU-L-2 is either slightly degraded or embedded with  $\text{PbI}_2$  inclusions. Figure 2(f) compares PL spectra of these two samples taken before the Raman measurement. SKKU-L-1 has higher peak intensity as well as longer peak wavelength than SKKU-L-2. In the PL spectrum of a typical semiconductor, the longer PL peak wavelength usually indicates the involvement of defects or impurities in the recombination. However, we find that for the hybrid

material the longer PL peak wavelength often indicates that the material is less degraded, which is further supported by the results of the SNU-c samples to be discussed later.

## 2. NREL-p samples

Figure 3 shows the Raman and PL spectra of a NREL-p sample. Figure 3(a) compares two spectra taken under the same low-excitation density and total acquisition time ( $\text{D}_{4_{100\times}}/800\text{ s}$ ) but with different CT/IT combinations, 1 s/4 s first, followed with 0.5 s/0.5 s. Clearly, the shorter interruption yields a more apparent  $100\text{-cm}^{-1}$  feature or less  $550\text{-cm}^{-1}$  band. Although  $\text{D}_{4_{100\times}}/800\text{ s}/0.5\text{ s}/0.5\text{ s}$  is found to be “safe” for SKKU-p-1, one should be alerted that the “safe” condition depends on the sample condition. The difference seems to indicate that the small domains are more sensitive to the illumination than the large ones, possibly due to the lower thermal conductivity and thus slower heat dissipation associated with the small polycrystalline domains, and/or the difference in surface effect. Figure 3(b) shows the excitation density dependence in the same conditions as in Fig. 2(d) for SKKU-p-1: the  $\sim 100\text{-cm}^{-1}$  feature becomes more and more apparent under  $\text{D}_3/400\text{ s}/0.5\text{ s}/0.5\text{ s}$  and  $\text{D}_2/100\text{ s}/0.5\text{ s}/0.5\text{ s}$ . These results are qualitatively consistent with those from the SKKU-p-1 sample, although there are no individually resolved peaks near  $100\text{ cm}^{-1}$  in this sample. After the D2 Raman measurement, the  $\text{D}_{4_{100\times}}/800\text{ s}/1\text{ s}/4\text{ s}$  measurement is repeated again, and the spectrum appears to be nearly the same as the initial one, as shown in Fig. 3(c), indicating no significant permanent structure transformation in this case. PL is measured using both a 442- and 532-nm laser at D4 with  $\text{TAT} = \text{CT} = 1\text{ s}$  before and after the first and last Raman spectrum measurement, as shown in Fig. 3(d). We note that the PL peak wavelength of the NREL-p sample ( $\sim 764$  nm) tends to be slightly shorter than that of the nondegraded SKKU samples. As shown in Fig. 3(d), although the PL peak positions show no or little change, the intensities have reduced significantly. We did not wait for a longer time to check if the intensity could recover, as partial recovery was reported in Ref. [30] after 12 h. Nevertheless, no PL emission near the  $\text{PbI}_2$  band gap is observed before and after the D2 Raman measurement. We note that in the NREL-p sample, even under  $\text{D}_{4_{100\times}}/800\text{ s}/1\text{ s}/4\text{ s}$ , the  $\sim 550\text{-cm}^{-1}$  band is not as prominent as in SKKU-p-1, rather it is comparable to that in SKKU-p-2, which seems to suggest that the sample is slightly degraded, possibly because the further reduced polycrystalline domain size in this sample makes it even less stable. This observation might explain why the previous reports also did not show the  $\sim 550\text{-cm}^{-1}$  band [27–30].

## 3. SNU-c samples

We now examine the single crystal sample SNU-c with results given in Fig. 4. Figure 4(a) contrasts two

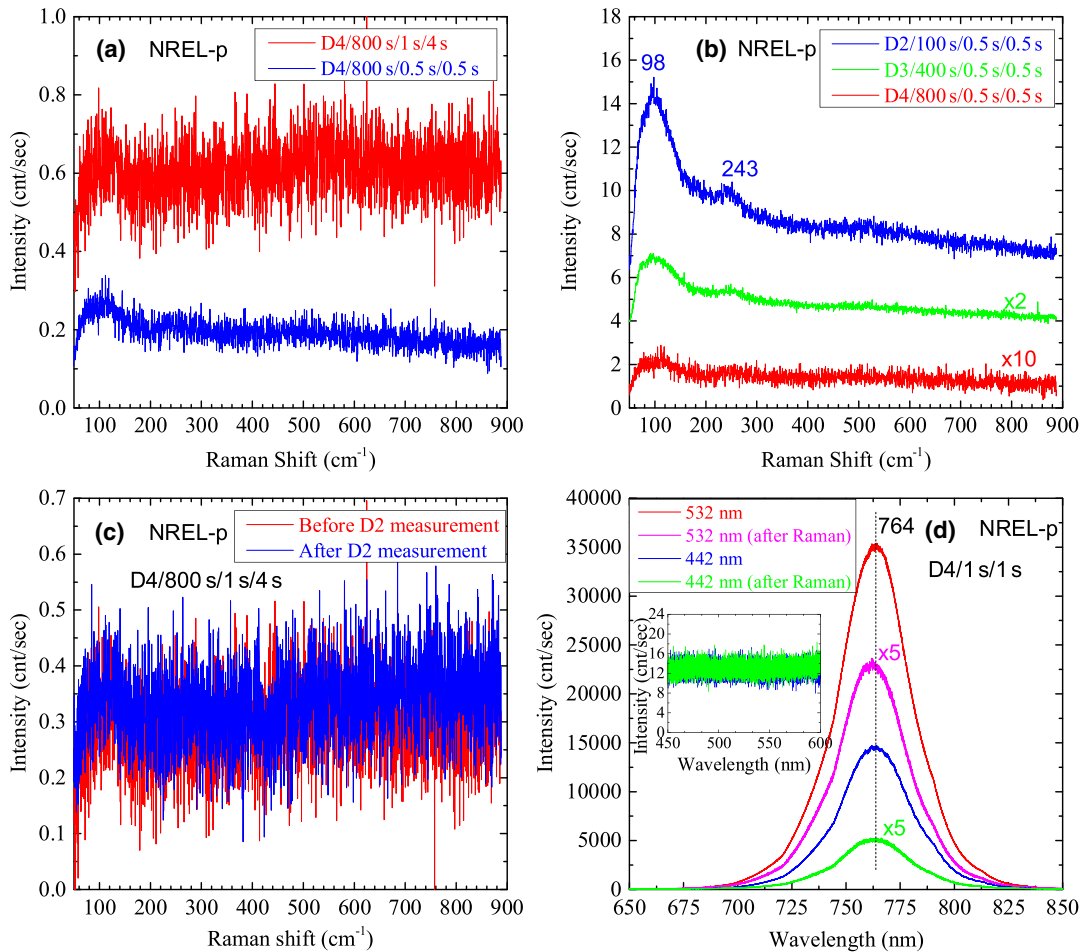


FIG. 3. Raman and PL spectra of NREL-p samples measured at different conditions. (a) D4 Raman spectra measured with different interruptions. (b) Raman spectra measured under different excitation density D4–D2. (c) D4/800 s/1 s/4 s measurements before and after the measurements shown in (b). (d) PL spectra measured before and after all the Raman measurements, using both a 442- and a 532-nm laser.

D4<sub>50×L</sub>/1600 s/0.5 s/0.5 s Raman spectra taken between one D2<sub>50×L</sub>/200 s/10 s/0.2 s measurement. While the D2 spectrum shows a visible  $\sim 100\text{-cm}^{-1}$  peak, the two D4 spectra are nearly the same, indicating that the D2<sub>50×L</sub>/100 s/0.5 s/0.5 s illumination does not cause irreversible change. However, in Fig. 4(b), after increasing the D2 illumination time, with one D2<sub>50×L</sub>/800 s/20 s/0.2 s followed by another D2<sub>50×L</sub>/100 s/0.5 s/0.5 s, in the repeated D4 spectrum the  $100\text{-cm}^{-1}$  peak now becomes somewhat visible, indicating that the longer D2 illumination does induce some structural change. Also, the D2 spectra are rather different between Figs. 4(a) and 4(b); i.e., longer D2 illumination has resulted in a more prominent  $\sim 100\text{-cm}^{-1}$  peak, a much reduced  $\sim 550\text{-cm}^{-1}$  band, and the appearance of a broad peak near  $250\text{ cm}^{-1}$ . In fact, the D2 spectra in Fig. 4(b) are similar to those in Fig. 3(b) for the NREL-p sample. Figure 4(c) shows the same measurements of Fig. 4(a), but the measured spot is flashed by D1 after the first D4 measurement. Now even at D4 major irreversible structure change is evident with the appearance

of multiple peaks related to PbI<sub>2</sub>. Figure 4(d) compares the PL spectra excited by 442 nm under D4<sub>50×L</sub>/1 s/1 s before and after the D4 Raman of Fig. 4(b) or 4(c). After the moderately strong illumination, D2<sub>50×L</sub>/800 s/20 s/0.2 s, the PL spectrum shows a small redshift and small intensity enhancement, indicating that the material remains in the hybrid structure despite some subtle structural change; whereas after being flashed with D1, the PL spectrum reveals a factor of 88 reduction in the peak intensity and a 24-nm redshift in the peak position, indicating major structure modification. To remove the uncertainty of the extremely weak signal under the D4 excitation, another test is done under D2. The results shown in Fig. 4(e) indicate that the  $\sim 100\text{-cm}^{-1}$  peak appears only under D2<sub>50×L</sub>/200 s/10 s/0.2 s and not under D2<sub>50×L</sub>/100 s/0.5 s/0.5 s, with the presence of the  $550\text{-cm}^{-1}$  band in both cases. These two spectra resemble, respectively, those of SKKU-p-1 and SKKU-p-2 in Fig. 2(a). The results of this single crystal sample again confirm the conclusion about the intrinsic Raman

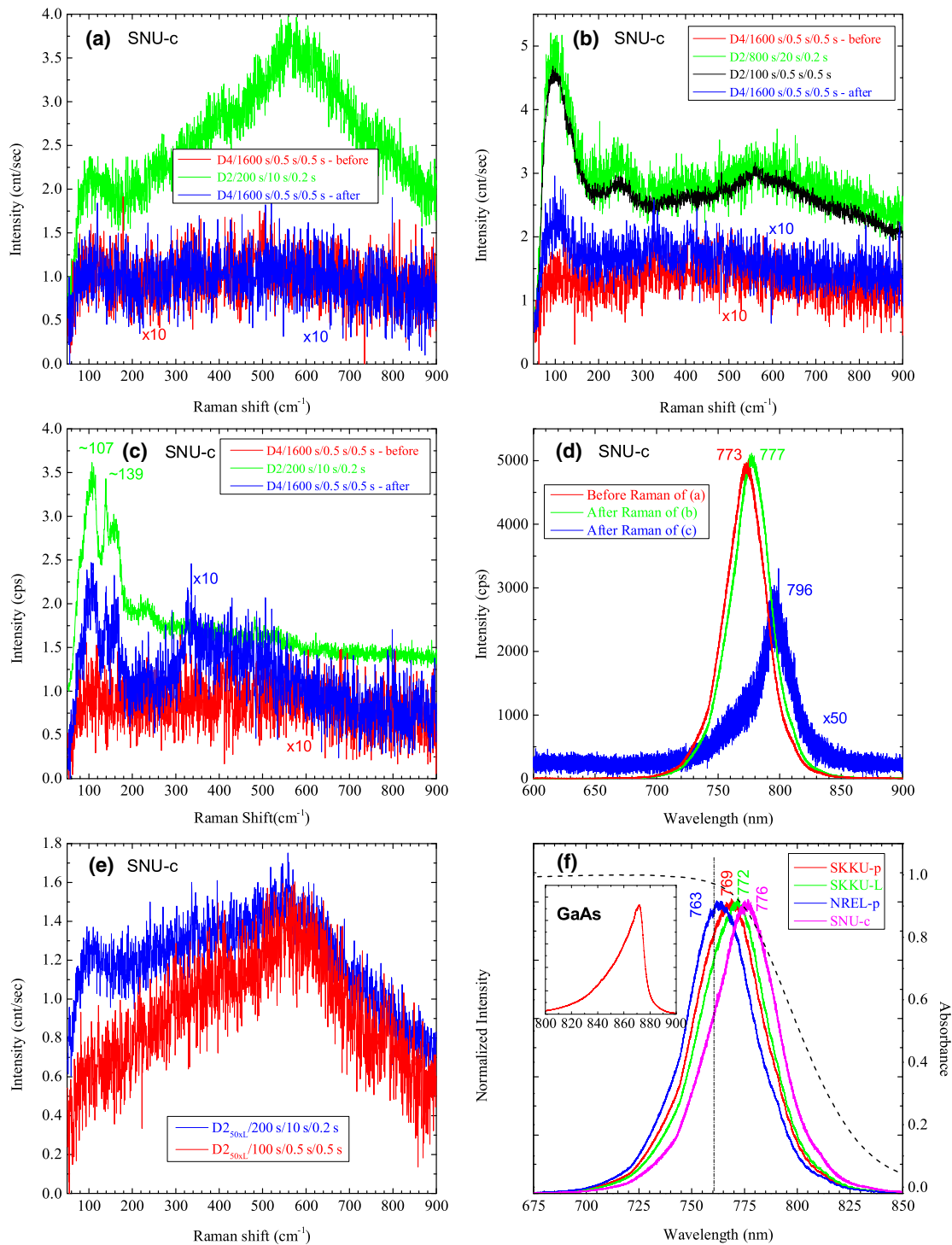


FIG. 4. Raman and PL spectra of SNU-c samples measured at different conditions. (a)–(c) Low-excitation density (D4) Raman spectra measured before and after different higher excitation density measurements. (d) D4 PL spectra measured before the Raman measurement shown in (a) and after the Raman measurements shown in (b) and (c). (e) Raman spectra measured at a moderately high excitation density D2 under different data collection conditions. (f) Comparison of the D4 PL spectra for four types of samples, SKKU-p, SKKU-L, NREL-p, and SNU-c, and an absorption spectrum of a SNU-c sample. The inset shows a room-temperature GaAs PL spectrum.

spectrum of the material derived from the polycrystalline samples.

The results shown above offer a consistent understanding of the intrinsic Raman characteristic of the MAPbI<sub>3</sub> hybrid

structure. Although the Raman modes associated with the PbI<sub>2</sub> cluster in the hybrid are expected to appear in a similar spectral range as in the bulk PbI<sub>2</sub> with the same nearest-neighbor configuration (PbI<sub>6</sub>), as shown theoretically

[27,31], the Raman cross sections for these modes appear to be very small, possibly due to the symmetry selection rule [22], as well as the inhomogeneous broadening, compared to the higher frequency modes that are likely associated with the MA molecules [23,27,31]. Therefore, a more comprehensive theoretical treatment including the disordering effect is required to interpret the intrinsic Raman spectrum.

Turning to the PL spectra, our results clearly reveal a significant and systematic variation in the peak position between the four sample types in their most pristine states, as evident by the direct comparison of their PL spectra in Fig. 4(f). The trend seems to be that the peak wavelength redshifts with increasing domain size, which is qualitatively consistent with the previously reported difference between the “meso” and “flat” sample (which differed in domain size) [28]. However, since in none of these cases the domain size was small enough for the quantum confinement effect to be significant, the peak wavelength shift is rather interesting. Since the small domain samples clearly exhibited strong structural disorder, i.e., no visible excitonic absorption peak even at low temperatures [41], the PL peak position and line shape largely reflect the density of states of the system. For the large domain or single crystalline samples, the excitonic band gaps could be unambiguously identified at low temperatures [41,42]. However, at room temperature it has been smeared out due to inhomogeneous broadening and could only be estimated to be around 1.63–1.64 eV or 760–756 nm [26,28,41,42], suggesting that significant disorder remains even in the large domain samples, as implied by the pseudotetragonal structure [15]. The room-temperature PL linewidths are in the range of 80 to 100 meV with a nearly symmetric energy distribution, which is significantly different from a semiconductor like GaAs exhibiting an asymmetric PL line shape with the higher energy side approximately following a Boltzmann distribution [inset of Fig. 4(f)] [44]. In these hybrid samples, the PL peak positions are Stokes shifted with respect to the excitonic band gap, as in a semiconductor alloy with strong energy fluctuation. Therefore, using the PL peak position or Tauc plot, in particular the latter, to determine the band gap is either ambiguous or misleading [9,45].

## B. Photostability: Reversible and irreversible change and metastable state

Photostability of MAPbI<sub>3</sub> depends not only on the illumination power density, total illumination time, and interruption, but also on the crystalline domain size. Here, we further examine the photostability and reversibility of the photoinduced structure changes.

### 1. Multiple stages of photoinduced structure transformation

The structural transformation appears to have multiple stages. Stage I is the as-grown or pristine structure as

revealed by the Raman spectrum of SKKU-p-1 or SKKU-p-5 in Fig. 2(a) or of SNU-c in Fig. 4(e) under D<sub>250×L</sub>/100 s/0.5 s/0.5 s. This stage can be observed only under very carefully controlled measurement conditions, typically very low excitation density and/or short illumination time and no or minimal exposure to the ambient condition, also depending on the sample condition (e.g., domain size). It has largely been overlooked in previous studies. Under light illumination or with ambient exposure, the material can easily be transformed into stage II, which is indicated by the appearance of the “bump” near 100 cm<sup>-1</sup> and simultaneous reduction of the 550-cm<sup>-1</sup> band, as represented by the spectrum of SKKU-p-2 in Fig. 2(a), of SKKU-L-1 in Fig. 2(e), of NREL-p in Fig. 3(a), and of SNU-c under D<sub>250×L</sub>/200 s/10 s/0.2 s in Fig. 4(a) or 4(e). Although the material can enter this stage either due to slight natural degradation or photo-induced transformation, there is a delicate difference between the natural degradation and phototransformation: namely, for the latter the material is in an excited state, which is less stable than the ground state. Even this stage was rarely observed in the literature, perhaps with an exception of Ref. [29], although there without the 550-cm<sup>-1</sup> band. In stage III, distinct Raman peaks become observable near 100 cm<sup>-1</sup>, as shown by SKKU-p-3 in Fig. 2(b) and SKKU-p-1 under higher excitation densities in Fig. 2(d) or SKKU-L-2 in Fig. 2(e). The Raman features of this stage seem to be in general agreement with those reported in the literature, such as Refs. [27–30], despite some variations in the exact peak positions, which are sensitive to the sample condition as well as the measurement condition. In stage IV, the typical Raman spectrum is like that of SKKU-p-4 in Fig. 2(b), which is essentially the same as that of PbI<sub>2</sub> and also very similar to those reported hybrid spectra measured under high excitation density [31,32]. Stage I appears to be a stable state at room temperature, although likely with a very small formation energy. The photoinduced transformation from stage I toward stage II has been shown to be reversible, as shown in Fig. 4(a), if the illumination power and time are very carefully controlled. There might be a small energy barrier between stage I and stage II. Stage II appears to be a metastable state, in the sense that it can endure some change towards stage III yet is reversible as long as it does not reach stage III, as we discuss below. However, the photoinduced transformation from stage II to stage III and thereafter is irreversible.

The phototransformation is accumulative with consecutive illuminations, as demonstrated by the results shown in Fig. 5. Figure 5(a) depicts 17 spectra of a SKKU-p sample, which is a fresh sample and had not been illuminated before, measured under D<sub>250×L</sub>/10 s/0.5 s/0.5 s with a ~20-s interval between the adjacent measurements, except for no. 0 under D<sub>250×L</sub>/1.5 s/0.5 s/0.5 s. The no. 0 spectrum indicates the sample was already in stage II at

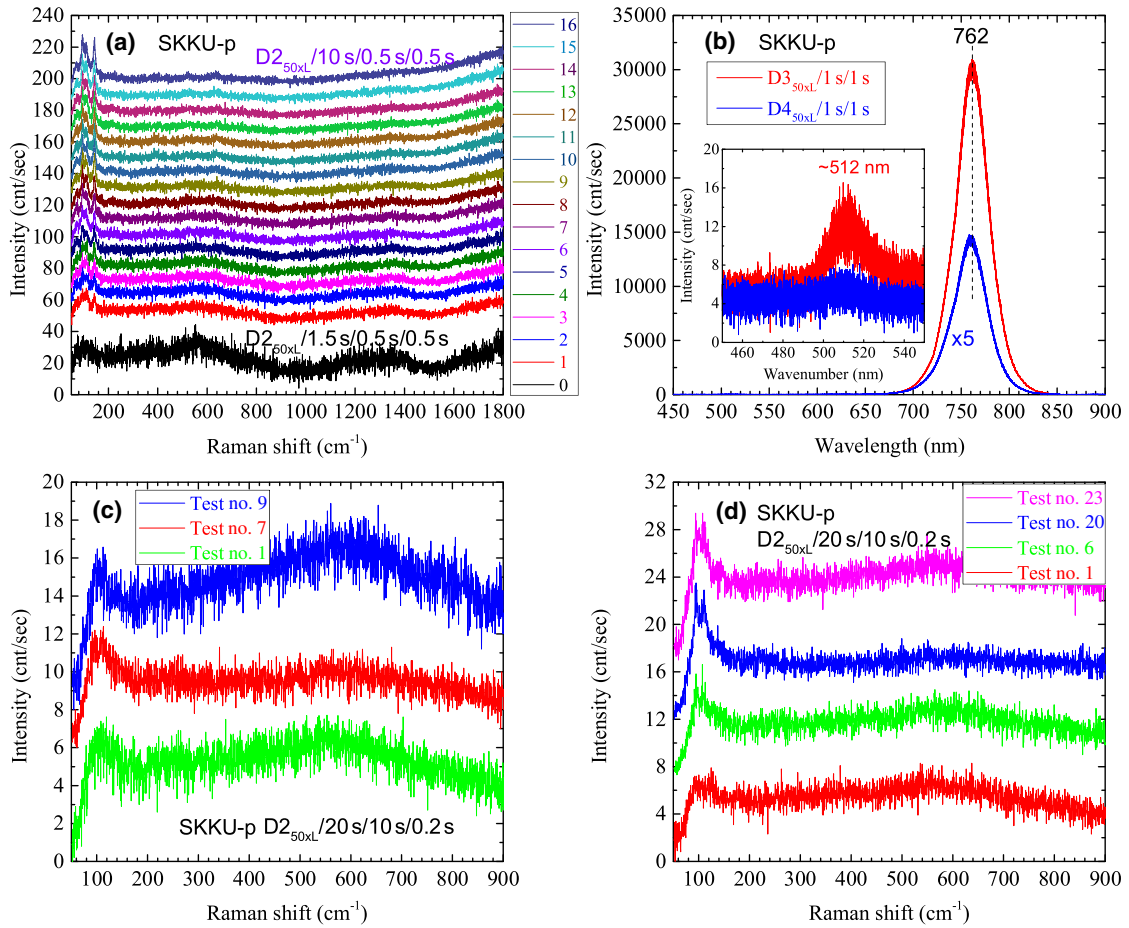


FIG. 5. Effects of multiple consecutive Raman measurements in SKKU-p samples under D2 excitation. (a) Sixteen consecutive measurements with  $\sim 20$  s in between. (b) PL spectra measured after the Raman measurements shown in (a). (c) Eight consecutive measurements with  $\sim 20$  s in between, then waited for 10 min before the last one (no. 9). (d) Twenty-two consecutive measurements with  $\sim 20$  s in between, then waited for 10 min before the last one (no. 23).

the beginning. With increasing the repeating number, the measured point quickly evolves into stage III then stage IV. Accompanying the appearance of multiple resolved peaks near  $100\text{ cm}^{-1}$ , the  $550\text{-cm}^{-1}$  band, as well as another band near  $1340\text{ cm}^{-1}$  that always accompanies the  $550\text{-cm}^{-1}$  band, systematically reduces. At the end of these Raman measurements, PL spectra are measured under  $D4_{50\times L}/1\text{ s}/1\text{ s}$  and  $D3_{50\times L}/1\text{ s}/1\text{ s}$ , as shown in Fig. 5(b). In comparison with the PL spectrum [similar to that of SKKU-p-1 in Fig. 2(c)] measured before the Raman measurements, the later PL spectra exhibit significant blueshift and major intensity reduction in the hybrid band gap peak, and the appearance of the  $\text{PbI}_2$  band gap emission. The photodegradation effect is qualitatively similar to the natural degradation, as shown in Fig. 2(c), but as an accelerated process. Typically, once the material enters stage III under illumination, the transformation becomes irreversible. To confirm this, two additional tests were carried out, with, respectively, 8 and 22 consecutive measurements under  $D2_{50\times L}/20\text{ s}/10\text{ s}/0.2\text{ s}$  with  $\sim 20\text{-s}$  interruption in between, then we waited for 10 min to take

the final measurement (no. 9 and no. 23, respectively). The results of the first test are shown in Fig. 5(c), indicating the material is mostly recovered (no. 1 versus no. 9), despite the fact that some change is induced during the test, for instance, the intensity variation of the  $550\text{-cm}^{-1}$  peak between no. 1 and no. 7. However, the second test yields irreversible change from stage II to stage III, as shown in Fig. 5(d), including the spectra of no. 1, no. 6, no. 20, and no. 23, where starting from no. 6 individual Raman peaks emerge in the  $100\text{-cm}^{-1}$  region. Note that there are some variations in the photodegradation threshold between the individual spots of the three tests, reflecting inhomogeneity of the polycrystalline film. This fluctuation becomes more apparent when a relatively high power, like D2, is used, because D2 can very easily drive the system from stage II to stage III.

The above-described phototransformation has also been observed in the single crystalline sample SNU-c in a qualitatively similar manner. Figure 6 shows the illumination time and pattern dependence and spatial variation of a SNU-c sample. Figures 6(a) and 6(b) contrast two extreme

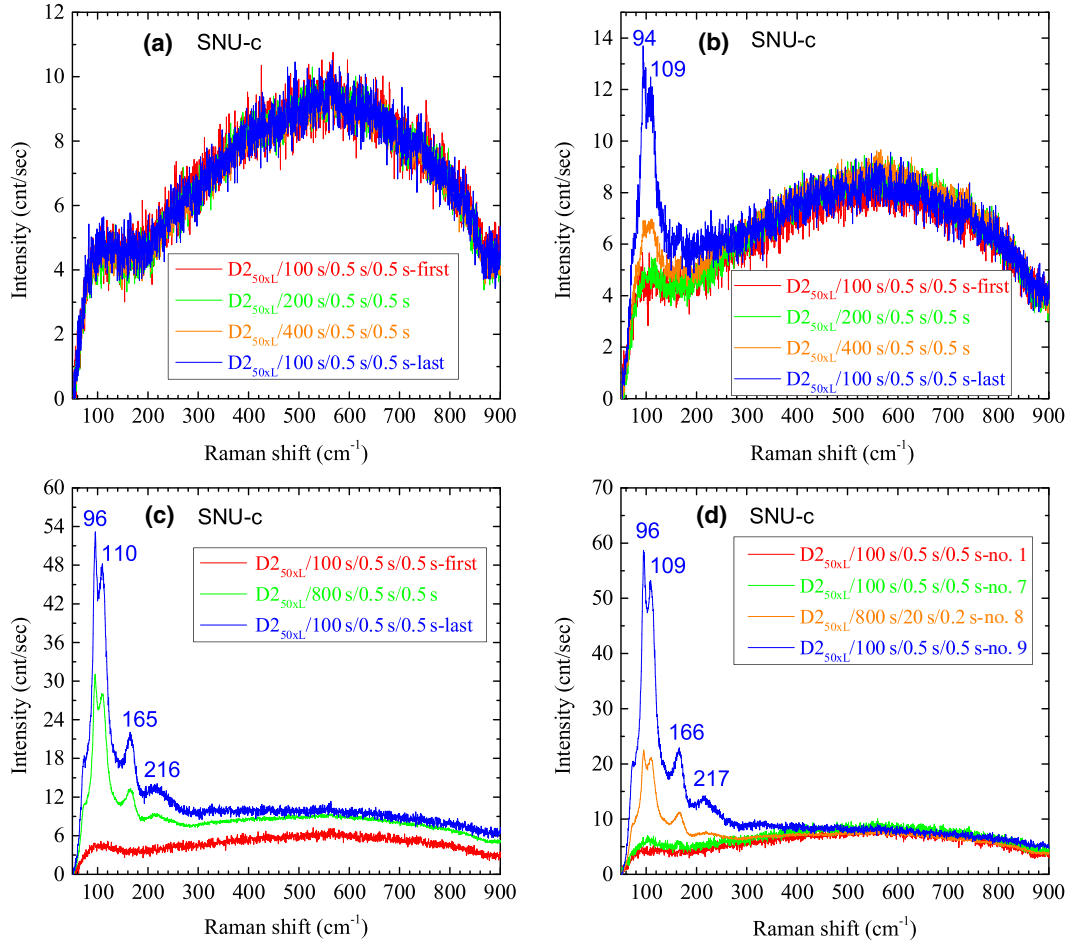


FIG. 6. Effects of multiple consecutive Raman measurements in SNU-c samples under D2 excitation. Panels (a) and (b) show spatial inhomogeneity. Panels (c) and (d) show the effect of long illumination time.

situations due to sample inhomogeneity observed from two spatial points each with four consecutive measurements. The first and last measurements under  $D2_{50\times L}/100\text{ s}/0.5\text{ s}/0.5\text{ s}$  alone usually would not lead to permanent change, according to the results of Figs. 4(a) and 4(c); thus, they are used as probing measurements. The two longer measurements in between (total 600-s illumination time) are used to induce change. In one case, Fig. 6(a), the first and the last spectra, as well as the two middle ones, are nearly the same. In the other relatively rare case or a weaker point on the sample, Fig. 6(b), the 100- $\text{cm}^{-1}$  region shows major enhancement and splitting starting from the third measurement, reflecting from stage II to stage III transformation. Two additional tests are performed on regular points. Figure 6(c) offers a test of three consecutive measurements using one single longer measurement in the middle,  $D2_{50\times L}/800\text{ s}/0.5\text{ s}/0.5\text{ s}$ , and the change in the last spectrum is significantly more pronounced than in Fig. 6(b). Figure 6(d) further shows another test: after an initial  $D2_{50\times L}/100\text{ s}/0.5\text{ s}/0.5\text{ s}$ , followed by eight alternating  $D2_{50\times L}/100\text{--}400\text{ s}/10\text{ s}/0.2\text{ s}$  and  $D2_{50\times L}/100\text{ s}/0.5\text{ s}/0.5\text{ s}$  measurements. Up to no. 7 (total

illumination time of 900 s from no. 2 to no. 7), the change is rather small; however, another  $D2_{50\times L}/800\text{ s}/10\text{ s}/0.2\text{ s}$  results in  $\text{PbI}_2$ -like Raman features similar to that of  $D2_{50\times L}/800\text{ s}/0.5\text{ s}/0.5\text{ s}$  in Fig. 6(c), and the last probing measurement under  $D2_{50\times L}/100\text{ s}/0.5\text{ s}/0.5\text{ s}$  yields a spectrum closer to that of  $\text{PbI}_2$  as SKKU-p-4 in Fig. 2(b). The results here indicate that under this particular excitation density, for a single crystalline sample, approximately 800-s illumination can result in irreversible structural degradation, and the effects of two different illumination patterns, 800 s/0.5 s/0.5 s and 800 s/10 s/0.2 s, are comparable.

## 2. Photostability and reversibility in photoluminescence

PL is often found more sensitive to the illumination than Raman, and thus more challenging to control and understand. Here, we examine more closely the light-induced changes in PL and reversibility of the effects, as well as the sample inhomogeneity using SKKU and SNU-c samples. It was reported that under weak illumination ( $0.1\text{ W}/\text{cm}^2 \sim 1\text{ sun}$ ) PL initially increased slightly then decreased very significantly, but recovered partially after

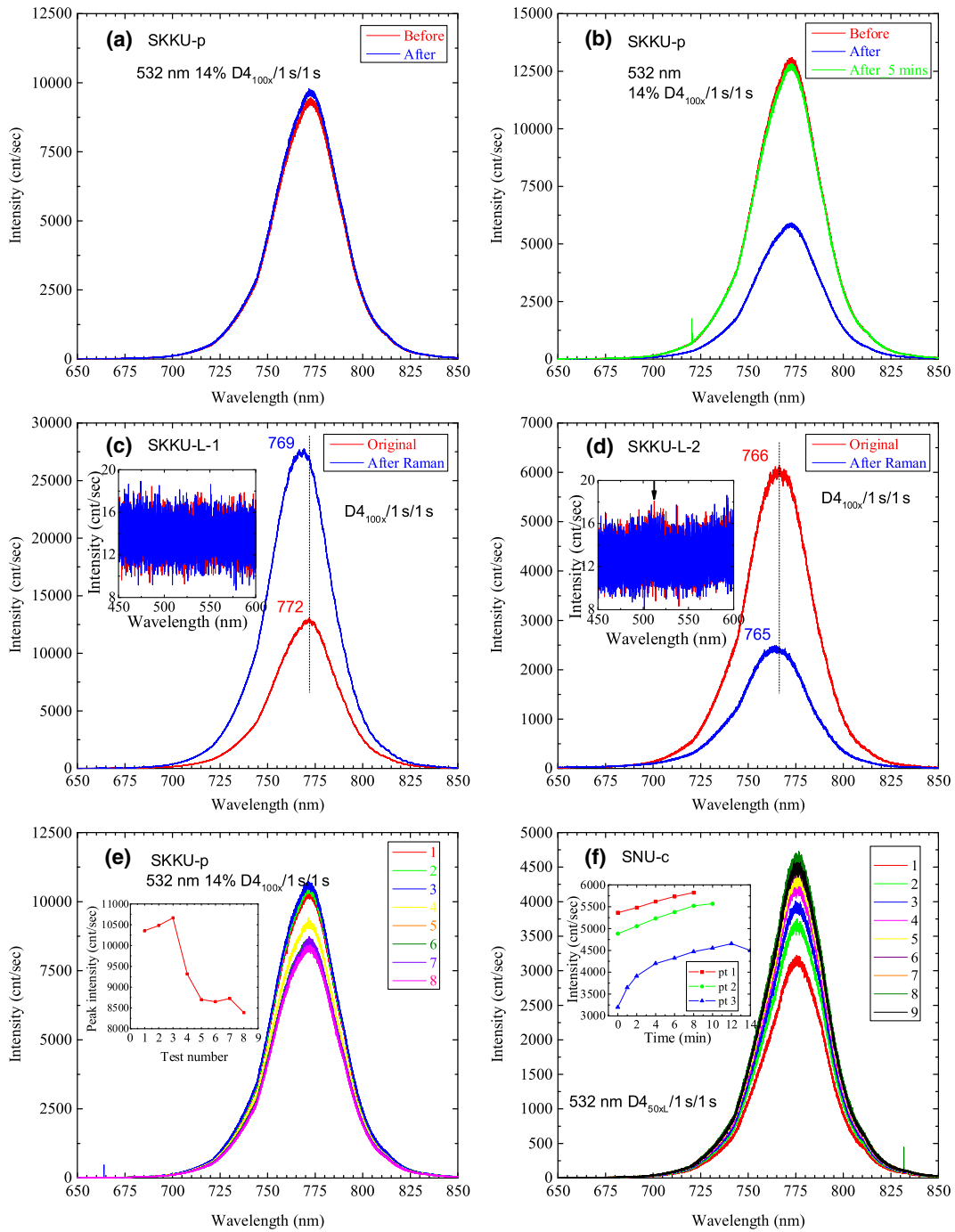


FIG. 7. Photo-stability of the PL spectra. (a) and (b) for two SKKU-p samples, low excitation density PL spectra before and after a higher power flash ( $\sim 1$  s). (c) and (d) for two SKKU-L samples, PL spectra measured before and after the Raman measurements shown in Fig. 2(e) and 2(f). (e) Consecutively measured PL spectra of a SKKU-p sample under very low excitation density. (f) Consecutively measured PL spectra of a SNU-c sample under very low excitation density.

12 h [30]. Based on the above Raman spectroscopy discussions, the sample there was likely already in stage III. We can now investigate the PL photostability of pristine (stage I) samples as well as somewhat degraded samples under different illumination conditions, with the results shown in Fig. 7.

*a. Brief high-power illumination*

We examine the effect of a brief moderate high-power (D3 or D2) illumination by measuring the low-power PL before and after the flash. The response on a fresh, stage I SKKU sample is found to be rather nonuniform: the change in peak intensity varies roughly from +60% to -60%.

If the intensity is found reduced, the same measurement is repeated again after 5 min. Two typical examples are given in Figs. 7(a) and 7(b), where the PL spectra are measured with the 532-nm laser under 14% of the  $D4_{100\times}$  power (14%  $D4_{100\times}/1$  s/1 s), before and after a flash (about 1 s) under 14% of the  $D3_{100\times}$  power. In Fig. 7(a), from one sample point, the change is minimal for the immediate repeat ( $\sim 20$ -s delay), whereas in Fig. 7(b), for another sample point, the immediate repeat exhibits a major reduction, but nearly full recovery after 5 min. However, not all reduced points could recover fully to the original intensity. We note a significant difference between the current work and the previous report [30]: there, the PL recovery time was found to be much longer (90% recovery after 12 h versus 20 s), which is likely due to the difference in sample condition (as hinted at by the difference in Raman spectra) as well as the excitation density (much higher in the current study). The findings suggest that the PL intensity change is not a reliable indicator of structural change. In fact, it is often not caused by any structure change, as we show below.

### *b. Prolonged low-power illumination*

We examine the effects of the relatively long Raman measurement on PL or multiple repeated PL measurements. Figures 7(c) and 7(d), respectively, compare the  $D4_{100\times}/1$  s/1 s PL spectra measured before and after the Raman spectra of SKKU-L-1 and SKKU-L-2 shown in Fig. 2(e) (under  $D4_{100\times}/1000$  s/1.25 s/3.75 s). For SKKU-L-1, with its Raman spectrum rather close to that of a pristine sample, the intensity of the hybrid peak is found to increase by about 108% plus a small blueshift after the Raman measurement, and no emission near the  $PbI_2$  band gap is visible. However, for SKKU-L-2, with its Raman spectrum showing weak  $PbI_2$  features, the PL intensity of the hybrid peak is already about 50% weaker than the other sample before the Raman measurement, and reduces further by about 57% after the Raman measurement, with a vestige of emission near the  $PbI_2$  band gap. It is apparent that the photostability depends on which degradation stage the sample initially was in.

We further examine the PL stability under repeated low-power measurements and the effect on the excitation density. For instance, on one location similar to that in Fig. 7(a), we find that eight consecutive measurements under 14% of D4 (14%  $D4_{100\times}/1$  s/1 s) yield a 20% reduction in the peak intensity, as shown in Fig. 7(e), whereas under 10% of D4 (10%  $D4_{100\times}/1$  s/1 s), the reduction is only 10%. However, the PL photostability is found to be significantly different in the SNU-c sample from that in the SKKU samples. In SNU-c, the PL intensity is found to increase with repeated measurements till it reaches a saturated value for nearly all measured locations, despite some variation in the overall intensity. Figure 7(f) depicts the spectra of multiple consecutive measurements

on one single spot under 532-nm  $D4_{50\times L}/1$  s/1 s, with intervals of 1 or 2 min, with the peak intensity versus measurement number shown in the inset for multiple locations.

These results indicate that both Raman and PL spectra are very sensitive to the sample degradation. However, Raman modes can more directly reflect the structure transformation, whereas the PL spectrum is not as easy to explain; in particular, the PL intensity has been found to exhibit either major enhancement or reduction under the condition (e.g.,  $D4/1$  s/1 s) at which structure transformation is not expected to occur. If PL is to be used for monitoring the structural change, the shift in peak position is perhaps more reliable, as shown, for example, in Figs. 4(d) and 7(c). PL intensity in a semiconductor is known to be sensitive to extrinsic effects such as defects and surface condition [10]. Therefore, it should be used with caution for monitoring the structure transformation.

### **3. More characteristics of partially and fully degraded samples**

We provide some further discussions on additional characteristics of partially and fully degraded or atypical hybrid samples, and attempt to clarify the differences between our own latest and previous results. These results can help to identify the characteristic spectral features of the (partially) degraded hybrid samples. The detailed descriptions and discussions are found in the Appendix, including Fig. 8, which summarizes the spectroscopy features of a few significant examples.

## **VI. SUMMARY AND CONCLUSIONS**

The organic-inorganic hybrid perovskite  $MAPbI_3$  is shown to be exceptionally easy to undergo structure transformation when being characterized using common spectroscopy techniques. By applying diligent controls in the measurement conditions, we are able to reveal the intrinsic spectroscopy signatures of the pristine samples, and characteristic spectroscopy features of degraded samples at different transformation stages, and we show that many of the previously reported Raman spectroscopy studies reflected partially degraded structures of different degrees. Importantly, despite the fact that a great variety of rather different Raman spectra have been observed either in this work or in the literature, they can be attributed to different stages of structure transformation and along different paths, e.g., relatively slow natural degradation of the ground state, photoinduced accelerated degradation of the excited state, and a combination of the two actions.

Intrinsic Raman spectrum of pristine  $MAPbI_3$  (stage I— a stable state with a small formation energy) should exhibit no visible discrete Raman modes in the spectral region of the primary Raman modes (around  $100\text{ cm}^{-1}$ ) of  $PbI_2$ , but a broad band peaked at around  $550\text{ cm}^{-1}$ . The appearance

TABLE I. Summary of Raman data in Figs. 1–6. The asterisk indicates a light-induced degradation state.

| Sample ID | Figure | Excitation density and numerical aperture | Total acquisition time (TAT) (s) | Data collection time (CT) (s) | Interruption time (IT) (s) | Comments                     |
|-----------|--------|---|----------------------------------|-------------------------------|----------------------------|------------------------------|
| SKKU-p-1  | 2(a)   | D4 100×                                   | 800                              | 0.5                           | 0.5                        | Stage I                      |
| SKKU-p-2  | 2(a)   | D4 100×                                   | 800                              | 0.5                           | 0.5                        | Stage II                     |
| SKKU-p-3  | 2(b)   | D4 50×                                    | 800                              | 0.5                           | 0.5                        | Stage III                    |
| SKKU-p-4  | 2(b)   | D4 100×                                   | 800                              | 0.5                           | 0.5                        | Stage IV                     |
| SKKU-p-5  | 2(a)   | D4 100×                                   | 1                                | 1                             | N/A                        | Stage I                      |
| SKKU-p-1  | 2(d)   | D4 100×                                   | 800                              | 0.5                           | 0.5                        | Stage I                      |
| SKKU-p-1  | 2(d)   | D3 100×                                   | 400                              | 0.5                           | 0.5                        | Stage III*                   |
| SKKU-p-1  | 2(d)   | D2 100×                                   | 100                              | 0.5                           | 0.5                        | Stage III*                   |
| SKKU-L-1  | 2(e)   | D4 100×                                   | 1000                             | 1.25                          | 3.75                       | Stage II                     |
| SKKU-L-2  | 2(e)   | D4 100×                                   | 1000                             | 1.25                          | 3.75                       | Stage III or stage I + IV    |
| NREL-p    | 3(a)   | D4 100×                                   | 800                              | 1                             | 4                          | Stage II                     |
| NREL-p    | 3(a)   | D4 100×                                   | 800                              | 0.5                           | 0.5                        | Stage II*                    |
| NREL-p    | 3(b)   | D4 100×                                   | 800                              | 0.5                           | 0.5                        | Stage II*                    |
| NREL-p    | 3(b)   | D3 100×                                   | 400                              | 0.5                           | 0.5                        | Stage II*                    |
| NREL-p    | 3(b)   | D2 100×                                   | 100                              | 0.5                           | 0.5                        | Stage II*                    |
| NREL-p    | 3(c)   | D4 100×                                   | 800                              | 1                             | 4                          | Stage II (before)            |
| NREL-p    | 3(c)   | D4 100×                                   | 800                              | 1                             | 4                          | Stage II (after)             |
| SNU-c     | 4(a)   | D4 50 × L                                 | 1600                             | 0.5                           | 0.5                        | Stage I (before)             |
| SNU-c     | 4(a)   | D2 50 × L                                 | 200                              | 10                            | 0.2                        | Stage II*                    |
| SNU-c     | 4(a)   | D4 50 × L                                 | 200                              | 10                            | 0.2                        | Stage I (after)              |
| SNU-c     | 4(b)   | D4 50 × L                                 | 1600                             | 0.5                           | 0.5                        | Stage I (before)             |
| SNU-c     | 4(b)   | D2 50 × L                                 | 800                              | 20                            | 0.2                        | Stage II*                    |
| SNU-c     | 4(b)   | D2 50 × L                                 | 100                              | 0.5                           | 0.5                        | Stage II*                    |
| SNU-c     | 4(b)   | D4 50 × L                                 | 1600                             | 0.5                           | 0.5                        | Stage III* (after)           |
| SNU-c     | 4(c)   | D4 50 × L                                 | 1600                             | 0.5                           | 0.5                        | Stage I (before)             |
| SNU-c     | 4(c)   | D2 50 × L                                 | 200                              | 10                            | 0.2                        | Stage III*                   |
| SNU-c     | 4(c)   | D4 50 × L                                 | 1600                             | 0.5                           | 0.5                        | Stage III* (after)           |
| SNU-c     | 4(e)   | D2 50 × L                                 | 100                              | 0.5                           | 0.5                        | Stage I                      |
| SNU-c     | 4(e)   | D2 50 × L                                 | 200                              | 10                            | 0.2                        | Stage II*                    |
| SKKU-p    | 5(a)   | D2 50 × L                                 | 1.5                              | 0.5                           | 0.5                        | Stage II (no. 0)             |
| SKKU-p    | 5(a)   | D2 50 × L                                 | 10                               | 0.5                           | 0.5                        | Stage III* or IV* (no. 1–16) |
| SKKU-p    | 5(c)   | D2 50 × L                                 | 20                               | 10                            | 0.2                        | Stage II (no. 1)             |
| SKKU-p    | 5(c)   | D2 50 × L                                 | 20                               | 10                            | 0.2                        | Stage II* (no. 7)            |
| SKKU-p    | 5(c)   | D2 50 × L                                 | 20                               | 10                            | 0.2                        | Stage II (no. 9)             |
| SKKU-p    | 5(d)   | D2 50 × L                                 | 20                               | 10                            | 0.2                        | Stage II (no. 1)             |
| SKKU-p    | 5(d)   | D2 50 × L                                 | 20                               | 10                            | 0.2                        | Stage III* (no. 6)           |
| SKKU-p    | 5(d)   | D2 50 × L                                 | 20                               | 10                            | 0.2                        | Stage III* (no. 20)          |
| SKKU-p    | 5(d)   | D2 50 × L                                 | 20                               | 10                            | 0.2                        | Stage III* (no. 23)          |
| SNU-c     | 6(a)   | D2 50 × L                                 | 100                              | 0.5                           | 0.5                        | Stage II* (first)            |
| SNU-c     | 6(a)   | D2 50 × L                                 | 200                              | 0.5                           | 0.5                        | Stage II*                    |
| SNU-c     | 6(a)   | D2 50 × L                                 | 400                              | 0.5                           | 0.5                        | Stage II*                    |
| SNU-c     | 6(a)   | D2 50 × L                                 | 100                              | 0.5                           | 0.5                        | Stage II* (last)             |
| SNU-c     | 6(b)   | D2 50 × L                                 | 100                              | 0.5                           | 0.5                        | Stage II* (first)            |
| SNU-c     | 6(b)   | D2 50 × L                                 | 200                              | 0.5                           | 0.5                        | Stage II*                    |
| SNU-c     | 6(b)   | D2 50 × L                                 | 400                              | 0.5                           | 0.5                        | Stage III*                   |
| SNU-c     | 6(b)   | D2 50 × L                                 | 100                              | 0.5                           | 0.5                        | Stage III* (last)            |
| SNU-c     | 6(c)   | D2 50 × L                                 | 100                              | 0.5                           | 0.5                        | Stage II* (first)            |
| SNU-c     | 6(c)   | D2 50 × L                                 | 800                              | 0.5                           | 0.5                        | Stage IV*                    |
| SNU-c     | 6(c)   | D2 50 × L                                 | 100                              | 0.5                           | 0.5                        | Stage IV* (last)             |
| SNU-c     | 6(d)   | D2 50 × L                                 | 100                              | 0.5                           | 0.5                        | Stage II* (no. 1)            |
| SNU-c     | 6(d)   | D2 50 × L                                 | 100                              | 0.5                           | 0.5                        | Stage II* (no. 7)            |
| SNU-c     | 6(d)   | D2 50 × L                                 | 800                              | 20                            | 0.2                        | Stage IV* (no. 8)            |
| SNU-c     | 6(d)   | D2 50 × L                                 | 100                              | 0.5                           | 0.5                        | Stage IV* (no. 9)            |

TABLE II. Summary of PL data. All PL spectra are measured under TAT/CT = 1 s/1 s. The asterisk indicates a light-induced degradation state.

| Sample ID | Figure | Excitation density and numerical aperture | Excitation source (nm) | Comment   |
|-----------|--------|---|------------------------|---|
| SKKU-p-1  | 2(c)   | D4 100×                                   | 442                    | Stage I   |
| SKKU-p-2  | 2(c)   | D4 100×                                   | 442                    | Stage II, little reduction in intensity   |
| SKKU-p-3  | 2(c)   | D4 50 × L                                 | 442                    | Stage III, major intensity reduction  |
| SKKU-p-4  | 2(c)   | D4 100×                                   | 442                    | Stage IV, appearance of PbI <sub>2</sub> peak   |
| SKKU-p-4  | 2(c)   | D4 100×                                   | 532                    | Stage IV, almost no perovskite emission   |
| SKKU-L-1  | 2(f)   | D4 100×                                   | 442                    | Stage II  |
| SKKU-L-2  | 2(f)   | D4 100×                                   | 442                    | Stage III or stage I + IV, intensity reduction and blue shift                           |
| NREL-p    | 3(d)   | D4 100×                                   | 532                    | Stage II (before)   |
| NREL-p    | 3(d)   | D4 100×                                   | 532                    | Stage II* (after), intensity reduction  |
| NREL-p    | 3(d)   | D4 100×                                   | 442                    | Stage II (before)   |
| NREL-p    | 3(d)   | D4 100×                                   | 442                    | Stage II* (after), intensity reduction  |
| SNU-c     | 4(d)   | D4 50 × L                                 | 442                    | Stage I (before a)  |
| SNU-c     | 4(d)   | D4 50 × L                                 | 442                    | Stage II* (after b), small enhancement and small red shift                              |
| SNU-c     | 4(d)   | D4 50 × L                                 | 442                    | Stage III* (after c), major intensity reduction and 24 nm redshift                      |
| SNU-c     | 4(f)   | D4 50 × L                                 | 442                    | Stage I   |
| NREL-p    | 4(f)   | D4 100×                                   | 442                    | Stage II  |
| SKKU-L    | 4(f)   | D4 100×                                   | 442                    | Stage II  |
| SKKU-p    | 4(f)   | D4 100×                                   | 442                    | Stage I   |
| SKKU-p    | 5(b)   | D4 50 × L                                 | 442                    | Stage III* or IV * Significant blueshift and major intensity reduction                  |
| SKKU-p    | 5(b)   | D3 50 × L                                 | 442                    | Stage III* or IV * with appearance of the PbI <sub>2</sub> band gap emission            |
| SKKU-p    | 7(a)   | 14% D4 100×                               | 532                    | Stage I (before)  |
| SKKU-p    | 7(a)   | 14% D4 100×                               | 532                    | Stage I (after), minimum change in intensity  |
| SKKU-p    | 7(b)   | 14% D4 100×                               | 532                    | Stage I (before)  |
| SKKU-p    | 7(b)   | 14% D4 100×                               | 532                    | Stage I (after), major intensity reduction  |
| SKKU-p    | 7(b)   | 14% D4 100×                               | 532                    | Stage I (after 5 min.), fully recovery  |
| SKKU-L-1  | 7(c)   | D4 100×                                   | 442                    | Stage II (original)   |
| SKKU-L-1  | 7(c)   | D4 100×                                   | 442                    | Stage II (after Raman), 108% intensity increment; no PbI <sub>2</sub> band gap          |
| SKKU-L-2  | 7(d)   | D4 100×                                   | 442                    | Stage III or Stage I + IV (original)  |
| SKKU-L-2  | 7(d)   | D4 100×                                   | 442                    | Stage IV (after Raman), intensity reduction; emission near the PbI <sub>2</sub> bandgap |
| SKKU-p    | 7(e)   | 14% D4 100×                               | 532                    | Stage I, no. 1–8, 20% reduction in intensity  |
| SNU-c     | 7(f)   | D4 50 × L                                 | 532                    | Stage I, no. 1–9, intensity increases till saturation                                   |

of a hump in the 100-cm<sup>-1</sup> region, accompanied by the intensity reduction of the 550-cm<sup>-1</sup> band, is the first indication of structure transformation into the next stage (stage II—a metastable state). The development from a hump to discrete Raman modes in the 100-cm<sup>-1</sup> region typically indicates the transformation into stage III, and is irreversible. Ammonia (NH<sub>3</sub>) intercalated PbI<sub>2</sub> could be one of the possible intermediate states. PbI<sub>2</sub> is usually the final product (stage IV) of the transformation. However, different intermediate states of stage III can lead to different final states, e.g., 2H-PbI<sub>2</sub> versus 4H-PbI<sub>2</sub>. A partially degraded sample may respond differently to light illumination from a pristine sample, for instance, the appearance of a Raman peak at around 250 cm<sup>-1</sup> that might not be observable if the initial state is stage I. The signature Raman features of different stages are universal for the MAPbI<sub>3</sub> samples of different crystalline domain sizes. However, in general, the photodegradation thresholds in terms of illumination time and/or power density seem to

increase with increasing domain size (on the order of NREL-p, SKKP-p, and SNU-c), which is likely due to the variation in the thermal conductivity and/or surface effect.

On the PL spectrum of MAPbI<sub>3</sub>, the structure transformation typically yields the intensity reduction and peak blueshift of the emission near the hybrid band gap. A severely degraded sample tends to yield emission near the band gap of the PbI<sub>2</sub>. Even at the measurement condition not expecting photoinduced structure transformation, PL intensity may exhibit significant instability, where the polycrystalline samples tend to show an inhomogeneous response to light illumination, for instance, exhibiting either enhanced or reduced PL intensity, PL quenching being either reversible or irreversible; but the single crystalline sample tends to show increasing PL intensity till saturation under repeated measurements. Therefore, the PL intensity change may or may not reflect the structural change. Relatively speaking, PL is a less reliable technique for monitoring the structure transformation compared to

TABLE III. Key spectroscopy characteristics of the four structure transformation stages.

| Stages   | Raman  | PL  |
|--|--|---|
| I. Pristine and stable state                   | No visible discrete Raman modes around $100\text{ cm}^{-1}$ but with a broad band at $\sim 550\text{ cm}^{-1}$ | Blueshift; peak intensity reduction; $\text{PbI}_2$ band edge PL peak appears at stage IV |
| II. Metastable state                           | Appearance of a hump in the $100\text{-cm}^{-1}$ region; reduction of the $550\text{-cm}^{-1}$ band            |   |
| III. Partially and irreversibly degraded state | Appearance of discrete Raman modes in the $100\text{-cm}^{-1}$ region, the $550\text{-cm}^{-1}$ band very weak |   |
| IV. Fully degraded state                       | Resembling $\text{PbI}_2$ Raman spectrum   |   |

Raman, which is more directly correlated with the crystalline structure.

Tables I and II summarize, respectively, the Raman and PL spectra shown in Figs. 2–7, including the basic sample information, measurement conditions, and approximate degradation stages and brief comments. Table III summarizes the key spectroscopy characteristics of the four stages.

### ACKNOWLEDGMENTS

The work at UNC-Charlotte was partially supported with funds from a Bissell Distinguished Professorship (Y.Z.); at SKKU by the National Research Foundation of Korea (NRF) grants funded by the Ministry of Science, ICT and Future Planning (MSIP) of Korea under Contracts No. NRF-2010-0014992, No. NRF-2012M1A2A2671721, No. NRF-2012M3A7B4049986 (Nano Material Technology Development Program), and No. NRF-2012M3A6A7054861 (Global Frontier R&D Program on Center for Multiscale Energy System); at NREL by the hybrid perovskite solar-cell program of the National Center for Photovoltaics funded by the U.S. Department of Energy, Office of Energy Efficiency and Renewable Energy, Solar Energy Technologies Office, for the work performed at the National Renewable Energy Laboratory (Contract No. DE-AC36-08-GO28308); at SNU by the National University Research Fund (GK261001009), the Changjiang Scholar and Innovative Research Team (IRT\_14R33), the Overseas Talent Recruitment Project (B14041), and the Chinese National 1000-talent-plan program (1110010341); at the Molecular Foundry by the Office of Science, Office of Basic Energy Sciences, U.S. Department of Energy, under Contract No. DE-AC02-05CH11231. Y.Z. thanks P. A. Beckmann for discussions about  $\text{PbI}_2$  polytypism and J. E. Spanier for discussions about Raman selection rules in perovskite structures.

Q. C. and H. L. contributed equally to this work.

### APPENDIX:

#### A. Different degradation products

We previously reported that there were substantial differences in Raman features between small and large crystalline domains in SKKU samples: the overall intensity

was much lower for SKKU-p, and additional features were observed in SKKU-L [38], as shown in Fig. 8(a). These spectra were obtained under  $\text{D}_{250\times\text{L}}/200\text{ s}/10\text{ s}/0.2\text{ s}$  with the 532-nm laser when the sample was first received (the color was dark). As it has now become apparent, these spectra likely reflect the degradation stage III, more so for the large domain, because of the photodegradation during the measurement. Interestingly, the highly degraded SKKU-L sample shows more features (e.g., 68, 101,  $\sim 143$ ,  $\sim 242$ ,  $\sim 316\text{ cm}^{-1}$ ) than that of 2H or 4H  $\text{PbI}_2$  [33,36]. Among these additional peaks, the  $143\text{ cm}^{-1}$  is from the  $\text{TiO}_2$  buffer layer (which we explain later). As a matter of fact, the overall spectrum resembles that of ammonia ( $\text{NH}_3$ ) intercalated  $\text{PbI}_2$  in the region below  $120\text{ cm}^{-1}$  [37]. If the spectrum reported in Ref. [37] is indeed of intrinsic to ammonia intercalated  $\text{PbI}_2$ , the SKKU-L spectrum in Fig. 8(a) could indicate that the ammonia intercalated  $\text{PbI}_2$  is an intermediate state of the photodegradation, which then points to a possible degradation path of the hybrid.

However, not all large domains exhibited the spectrum shown in Fig. 8(a); for instance, some did not show the 68- and  $101\text{-cm}^{-1}$  peaks. Those large domains that did and did not show these two peaks tended to result in two distinctly different spectra when further evolving into  $\text{PbI}_2$ . For comparison, Fig. 8(b) shows three representative Raman spectra measured from different locations on what appeared to be a fully degraded SKKU sample (i.e., completely turned yellow) under the same condition as in Fig. 8(a), but exhibiting significantly enhanced overall intensities. After degradation, those large hybrid domains typically turned into large  $\text{PbI}_2$  domains, although they somewhat shrank in size. There are two distinctly different types of spectra for the fully degraded large domains. One resembles that in Fig. 8(a), but with reduced splitting between the two lowest frequency peaks (approximately from 6 to  $3\text{ cm}^{-1}$ ) and reduced intensity of the  $316\text{-cm}^{-1}$  peak, referred to as SKKU-L-T1. The  $3\text{-cm}^{-1}$  splitting matches that of the  $E_g$  mode undergoing 2H to 4H transformation [33], which might suggest a transformation from ammonia intercalated  $\text{PbI}_2$  to 4H- $\text{PbI}_2$ . In the inset of Fig. 8(b), a comparison is made between a further degraded state from that in Fig. 8(a) and the final state. We note that the SKKU-L-T1 structure is stable in air, as measured 9 days later on the same domain.

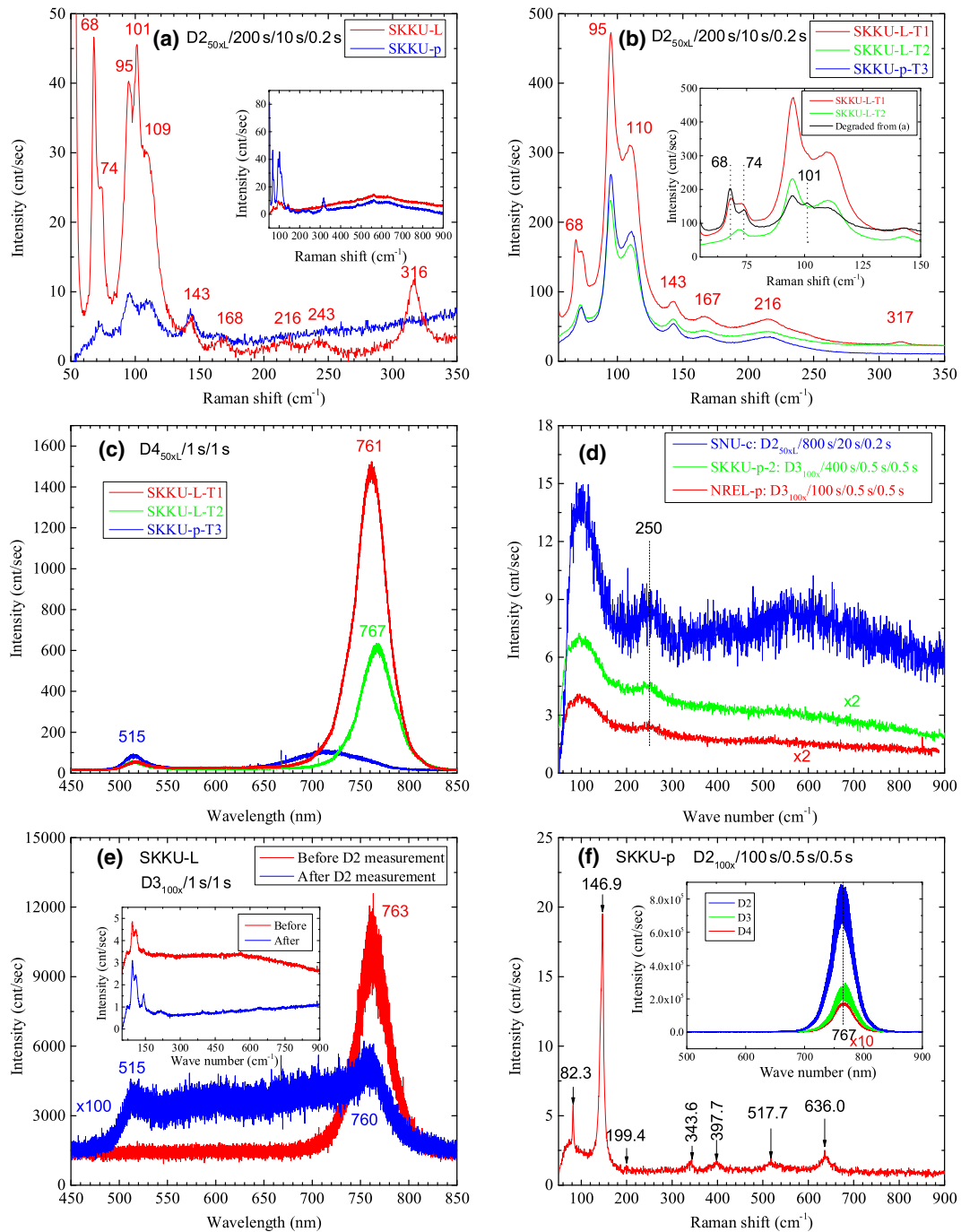


FIG. 8. Raman and PL spectra of partially or fully degraded samples. (a) Comparison of partially photodegraded SKKU sample between large and small domain (the inset shows the spectra in a larger spectral range). (b) Nearly fully degraded SKKU samples (including two distinctively different large domains), and the inset shows the spectra in a smaller spectral range. (c) PL spectra of the samples shown in (b). (d) The effect of photoinduced structure transformation in an already partially degraded sample due to the course of nature, showing a common Raman peak at around  $250\text{ cm}^{-1}$ . (e) PL spectra of a partially degraded SKKU-L sample measured before and after high-excitation density Raman measurement (the inset shows the corresponding Raman spectra). (f) Raman and PL spectra of an atypical location in a SKKU-p sample.

The other type, SKKU-L-T2, looks very similar to a small domain, SKKU-p-T3, in terms of both spectral features and their intensities. And they exhibit the same Raman features of  $2\text{H-PbI}_2$ .

It is interesting to compare the PL spectra of the three cases in Fig. 8(b), as shown in Fig. 8(c), all taken under  $442\text{-nm D4}_{50\times\text{L}}/1\text{ s}/1\text{ s}$ . The large domain samples show stronger IR peaks than the small domain. They have all

blueshifted with respect to the nondegraded sample and are at least a factor of 40–1000 weaker in magnitude than a typical nondegraded sample. In all of them, the  $\text{PbI}_2$  band gap emission peaks are clearly visible, with that of the small domain sample being the strongest. The results seem to suggest that the large domains, even after achieving nearly full conversion to  $\text{PbI}_2$ , might still contain some molecules perhaps in the form of defects in the structure. The remaining  $317\text{-cm}^{-1}$  Raman feature in the SKKU-L-T1 spectrum in Fig. 8(b) could be an indicator.

### B. Phototransformation of partially degraded materials

The photodegradation path depends on the degradation state in which the sample already is due to the natural degradation before the illumination. We note that the D4 spectrum of the NREL-p sample in Fig. 3(b) looks more like the slightly degraded SKKU-p-2 than the most pristine SKKU-p-1 in Fig. 2(a). The D2 or D3 spectrum of the NREL-p sample in Fig. 3(b) also appears to be different from those of the D2 or D3 spectrum of SKKU-p-1 (starting from the pristine state) in Fig. 2(d). However, we can find some common characteristic spectral features in weakly degraded samples of all three sources. Figure 8(d) compares the spectrum of NREL-p at  $\text{D3}_{100\times}/100\text{ s}/0.5\text{ s}/0.5\text{ s}$  from Fig. 3(b), of SKKU-p-2 at  $\text{D3}_{100\times}/400\text{ s}/0.5\text{ s}/0.5\text{ s}$ , and of SNU-c at  $\text{D2}_{50\times\text{L}}/800\text{ s}/20\text{ s}/0.2\text{ s}$  from Fig. 4(b). One can see a

new feature at around  $250\text{ cm}^{-1}$ , which was probably buried in the broad band near  $550\text{ cm}^{-1}$  in the less degraded samples, such as Figs. 2(d) and 4(a), and remained visible in the partially degraded large domain spectrum in Fig. 8(a). Note that this Raman band was also present in some previous reports [27,28], indicating that the results there likely represented partially degraded states. This comparison further supports the finding that despite the considerable variations in material synthesis and therefore the crystalline structures, the hybrid materials do share common structure transformation paths in the qualitative level.

Figure 8(e) shows an interesting PL spectrum of a severely degraded SKKU-L sample exhibiting a continuous emission spectrum from the  $\text{PbI}_2$  band gap to the hybrid band gap, in contrast to the spectrum measured from the same spot that was initially only mildly degraded before being subjected to a  $\text{D2}_{100\times}/100\text{ s}/0.5\text{ s}/0.5\text{ s}$  Raman measurement. The corresponding Raman spectra at  $\text{D4}_{100\times}/800\text{ s}/0.5\text{ s}/0.5\text{ s}$  before and after photoaccelerated degradation are included as the inset, which also reflects the transformation. The broad PL emission band expanding from near-infrared to green signifies a highly disordered transition phase between the hybrid perovskite and  $\text{PbI}_2$ .

Lastly, in Fig. 8(f), we show a “peculiar” or atypical Raman spectrum from one spot of a SKKU-p sample measured under  $\text{D2}_{100\times}/100\text{ s}/0.5\text{ s}/0.5\text{ s}$ . It shows two Raman modes at  $82$  and  $343\text{ cm}^{-1}$  that did not appear in the other hybrid samples, together with a set of Raman modes

TABLE IV. Summary of Raman data in Fig. 8. The asterisk indicates a light-induced degradation state.

| Sample ID | Figure | Excitation density and numerical aperture | Total acquisition time (s) | Data collection time (s) | Interruption time (s) | Comments                             |
|-----------|--------|---|----------------------------|--------------------------|-----------------------|--------------------------------------|
| SKKU-p    | 8(a)   | D2 $50 \times \text{L}$                   | 200                        | 10                       | 0.2                   | Stage III*                           |
| SKKU-L    | 8(a)   | D2 $50 \times \text{L}$                   | 200                        | 10                       | 0.2                   | Possibly intercalated $\text{PbI}_2$ |
| SKKU-L-T1 | 8(b)   | D2 $50 \times \text{L}$                   | 200                        | 10                       | 0.2                   | Stage IV* or 4H- $\text{PbI}_2$      |
| SKKU-L-T2 | 8(b)   | D2 $50 \times \text{L}$                   | 200                        | 10                       | 0.2                   | Stage IV* or 2H- $\text{PbI}_2$      |
| SKKU-p-T3 | 8(b)   | D2 $50 \times \text{L}$                   | 200                        | 10                       | 0.2                   | Stage IV* or 2H- $\text{PbI}_2$      |
| NREL-p    | 8(d)   | D3 $100 \times$                           | 100                        | 0.5                      | 0.5                   | Stage II*                            |
| SKKU-p-2  | 8(d)   | D3 $100 \times$                           | 400                        | 0.5                      | 0.5                   | Stage II*                            |
| SNU-c     | 8(d)   | D2 $50 \times \text{L}$                   | 800                        | 20                       | 0.2                   | Stage II*                            |
| SKKU-p    | 8(f)   | D2 $100 \times$                           | 100                        | 0.5                      | 0.5                   | $\text{TiO}_2$                       |

TABLE V. Summary of PL data in Fig. 8. All PL spectra are measured under  $\text{TAT}/\text{CT} = 1\text{ s}/1\text{ s}$ . The asterisk indicates a light-induced degradation state.

| Sample ID | Figure | Excitation density and numerical aperture | Excitation source (nm) | Comment  |
|-----------|--------|---|------------------------|--|
| SKKU-L-T1 | 8(c)   | D4 $50 \times \text{L}$                   | 442                    | Stage IV* $\text{PbI}_2$ band gap emission; large domains show stronger IR peaks than the small domain     |
| SKKU-L-T2 | 8(c)   | D4 $50 \times \text{L}$                   | 442                    | Stage IV*  |
| SKKU-p-T3 | 8(c)   | D4 $50 \times \text{L}$                   | 442                    | Stage IV*  |
| SKKU-L    | 8(e)   | D3 $100 \times$                           | 442                    | Stage III (before)   |
| SKKU-L    | 8(e)   | D3 $100 \times$                           | 442                    | Stage IV (after Raman), highly disordered transition phase between the hybrid perovskite to $\text{PbI}_2$ |

of anatase TiO<sub>2</sub> at 146.9 (*E<sub>g</sub>*), 397.7 (*B<sub>1g</sub>*), (517.7) (*A<sub>g</sub>*), and 636 cm<sup>-1</sup> (*E<sub>g</sub>*) [46]. The TiO<sub>2</sub> related peaks are no surprise, as they exist in other degraded hybrid samples, such as those shown in Fig. 8(b) (not plotted), because the degraded samples are much more transparent for the 532-nm laser; thus, more Raman signals from the TiO<sub>2</sub> buffer layer could be detected. A subtle difference in the TiO<sub>2</sub> *E<sub>g</sub>* mode between this sample and those in Fig. 8(b) is noted: a blueshift from ~143.3 to ~147 cm<sup>-1</sup>, which can be explained by the TiO<sub>2</sub> grain size change (approximately from >30 to 8 nm) [47]. The PL spectra from this spot, shown as the inset of Fig. 8(f), under 442-nm D4 (D3, D2)<sub>100×/1 s/1 s</sub> are still like those of a typical hybrid sample, except for a blueshift in peak position compared to a nondegraded sample. The Raman and PL spectra in Fig. 8 are summarized in Tables IV and V respectively.

- 
- [1] A. Kojima, K. Teshima, Y. Shirai, and T. Miyasaka, *Organometal Halide Perovskites as Visible-Light Sensitizers for Photovoltaic Cells*, *J. Am. Chem. Soc.* **131**, 6050 (2009).
- [2] J.-H. Im, C.-R. Lee, J.-W. Lee, S.-W. Park, and N.-G. Park, *6.5% Efficient Perovskite Quantum-Dot-Sensitized Solar Cell*, *Nanoscale* **3**, 4088 (2011).
- [3] J. Burschka, N. Pellet, S.-J. Moon, R. Humphry-Baker, P. Gao, M. K. Nazeeruddin, and M. Gratzel, *Sequential Deposition as a Route to High-Performance Perovskite-Sensitized Solar Cells*, *Nature (London)* **499**, 316 (2013).
- [4] M. M. Lee, J. Teuscher, T. Miyasaka, T. N. Murakami, and H. J. Snaith, *Efficient Hybrid Solar Cells Based on Meso-Structured Organometal Halide Perovskites*, *Science* **338**, 643 (2012).
- [5] N. J. Jeon, J. H. Noh, Y. C. Kim, W. S. Yang, S. Ryu, and S. I. Seok, *Solvent Engineering for High-Performance Inorganic-Organic Hybrid Perovskite Solar Cells*, *Nat. Mater.* **13**, 897 (2014).
- [6] W. Nie, H. Tsai, R. Asadpour, J.-C. Blancon, A. J. Neukirch, G. Gupta, J. J. Crochet, M. Chhowalla, S. Tretiak, M. A. Alam, H.-L. Wang, and A. D. Mohite, *High-Efficiency Solution-Processed Perovskite Solar Cells with Millimeter-Scale Grains*, *Science* **347**, 522 (2015).
- [7] Z. Xiao, C. Bi, Y. Shao, Q. Dong, Q. Wang, Y. Yuan, C. Wang, Y. Gao, and J. Huang, *Efficient, High Yield Perovskite Photovoltaic Devices Grown by Interdiffusion of Solution-Processed Precursor Stacking Layers*, *Energy Environ. Sci.* **7**, 2619 (2014).
- [8] M. Gratzel, *The Light and Shade of Perovskite Solar Cells*, *Nat. Mater.* **13**, 838 (2014).
- [9] M. A. Green, Y. Jiang, A. M. Soufiani, and A. Ho-Baillie, *Optical Properties of Photovoltaic Organic-Inorganic Lead Halide Perovskites*, *J. Phys. Chem. Lett.* **6**, 4774 (2015).
- [10] T. H. Grofner, Y. Zhang, and M. W. Wanlass, *An Extended Defect as a Sensor for Free Carrier Diffusion in a Semiconductor*, *Appl. Phys. Lett.* **102**, 012114 (2013).
- [11] Q. Chen and Y. Zhang, *The Reversal of the Laser-Beam-Induced-Current Contrast with Varying Illumination Density in a Thin-Film Solar Cell*, *Appl. Phys. Lett.* **103**, 242104 (2013).
- [12] H. S. Nalwa, *Handbook of Organic-Inorganic Hybrid Materials and Nanocomposites* (American Scientific Publishers, Stevenson Ranch, California, 2003).
- [13] X. Y. Huang, J. Li, Y. Zhang, and A. Mascarenhas, *From 1D Chain to 3D Network: Tuning Hybrid II-VI Nanostructures and Their Optical Properties*, *J. Am. Chem. Soc.* **125**, 7049 (2003).
- [14] Y. Zhang, Z. Islam, Y. Ren, P. A. Parilla, S. P. Ahrenkiel, P. L. Lee, A. Mascarenhas, M. J. McNevin, I. Naumov, H. X. Fu, X. Y. Huang, and J. Li, *Zero Thermal Expansion in a Nanostructured Inorganic-Organic Hybrid Crystal*, *Phys. Rev. Lett.* **99**, 215901 (2007).
- [15] A. Poglitsch and D. Weber, *Dynamic Disorder in Methylammoniumtrihalogenoplumbates (II) Observed by Millimeter-Wave Spectroscopy*, *J. Chem. Phys.* **87**, 6373 (1987).
- [16] Y. Zhang and L.-W. Wang, *Global Electronic Structure of Semiconductor Alloys through Direct Large-Scale Computations for III-V Alloys Ga<sub>x</sub>In<sub>1-x</sub>P*, *Phys. Rev. B* **83**, 165208 (2011).
- [17] B. Jusserand and M. Cardona, in *Light Scattering in Solids*, edited by M. Cardona and G. Güntherodt (Springer, Berlin, 1989), p. 49.
- [18] A. Mascarenhas, H. Cheong, and F. Alsina, in *Spontaneous Ordering in Semiconductor Alloys*, edited by A. Mascarenhas (Kluwer Academy, New York, 2002), p. 391.
- [19] S. Hirotsu, *Far-Infrared Reflectivity Spectra of CsPbCl<sub>3</sub>*, *Phys. Lett.* **41A**, 55 (1972).
- [20] D. M. Calistru, L. Mihut, S. Lefrant, and I. Baltog, *Identification of the Symmetry of Phonon Modes in CsPbCl<sub>3</sub> in Phase IV by Raman and Resonance-Raman Scattering*, *J. Appl. Phys.* **82**, 5391 (1997).
- [21] W. G. Nilsen and J. G. Skinner, *Raman Spectrum of Strontium Titanate*, *J. Chem. Phys.* **48**, 2240 (1968).
- [22] M. A. Islam, J. M. Rondinelli, and J. E. Spanier, *Normal Mode Determination of Perovskite Crystal Structures with Octahedral Rotations: Theory and Applications*, *J. Phys. Condens. Matter* **25**, 175902 (2013).
- [23] A. Maalej, Y. Abid, A. Kallel, A. Daoud, A. Lautié, and F. Romain, *Phase Transitions and Crystal Dynamics in the Cubic Perovskite CH<sub>3</sub>NH<sub>3</sub>PbCl<sub>3</sub>*, *Solid State Commun.* **103**, 279 (1997).
- [24] H. M. Cheong, A. Mascarenhas, P. Ernst, and C. Geng, *Effects of Spontaneous Ordering on Raman Spectra of GaInP*, *Phys. Rev. B* **56**, 1882 (1997).
- [25] C. C. Stoumpos, C. D. Malliakas, and M. G. Kanatzidis, *Semiconducting Tin and Lead Iodide Perovskites with Organic Cations: Phase Transitions, High Mobilities, and Near-Infrared Photoluminescent Properties*, *Inorg. Chem.* **52**, 9019 (2013).
- [26] Y. Liu, Z. Yang, D. Cui, X. Ren, J. Sun, X. Liu, J. Zhang, Q. Wei, H. Fan, F. Yu, X. Zhang, C. Zhao, and S. Liu, *Two-Inch-Sized Perovskite CH<sub>3</sub>NH<sub>3</sub>PbX<sub>3</sub> (X = Cl, Br, I) Crystals: Growth and Characterization*, *Adv. Mater.* **27**, 5176 (2015).
- [27] C. Quarti, G. Grancini, E. Mosconi, P. Bruno, J. M. Ball, M. M. Lee, H. J. Snaith, A. Petrozza, and F. D. Angelis, *The Raman Spectrum of the CH<sub>3</sub>NH<sub>3</sub>PbI<sub>3</sub> Hybrid*

- Perovskite: Interplay of Theory and Experiment*, *J. Phys. Chem. Lett.* **5**, 279 (2014).
- [28] G. Grancini, S. Marras, M. Prato, C. Giannini, C. Quarti, F. De Angelis, M. De Bastiani, G. E. Eperon, H. J. Snaith, L. Manna, and A. Petrozza, *The Impact of the Crystallization Processes on the Structural and Optical Properties of Hybrid Perovskite Films for Photovoltaics*, *J. Phys. Chem. Lett.* **5**, 3836 (2014).
- [29] M. Ledinský, P. Löper, B. Niesen, J. Holovský, S.-J. Moon, J.-H. Yum, S. De Wolf, A. Fejfar, and C. Ballif, *Raman Spectroscopy of Organic-Inorganic Halide Perovskites*, *J. Phys. Chem. Lett.* **6**, 401 (2015).
- [30] R. Gottesman, L. Gouda, B. S. Kalanoor, E. Haltzi, S. Tirosh, E. Rosh-Hodesh, Y. Tischler, A. Zaban, C. Quarti, E. Mosconi, and F. De Angelis, *Photoinduced Reversible Structural Transformations in Free-Standing CH<sub>3</sub>NH<sub>3</sub>PbI<sub>3</sub> Perovskite Films*, *J. Phys. Chem. Lett.* **6**, 2332 (2015).
- [31] B.-w. Park, S. M. Jain, X. Zhang, A. Hagfeldt, G. Boschloo, and T. Edvinsson, *Resonance Raman and Excitation Energy Dependent Charge Transfer Mechanism in Halide-Substituted Hybrid Perovskite Solar Cells*, *ACS Nano* **9**, 2088 (2015).
- [32] S. T. Ha, X. Liu, Q. Zhang, D. Giovanni, T. C. Sum, and Q. Xiong, *Synthesis of Organic-Inorganic Lead Halide Perovskite Nanoplatelets: Towards High-Performance Perovskite Solar Cells and Optoelectronic Devices*, *Adv. Opt. Mater.* **2**, 838 (2014).
- [33] R. Zallen and M. L. Slade, *Inter-Polytype Conversion and Layer-Layer Coupling in PbI<sub>2</sub>*, *Solid State Commun.* **17**, 1561 (1975).
- [34] V. Capozzi, A. Fontana, M. P. Fontana, G. Mariotto, M. Montagna, and G. Viliani, *Raman Scattering in PbI<sub>2</sub>*, *Nuovo Cimento Soc. Ital. Fis.* **39**, 556 (1977).
- [35] W. M. Sears, M. L. Klein, and J. A. Morrison, *Polytypism and the Vibrational Properties of PbI<sub>2</sub>*, *Phys. Rev. B* **19**, 2305 (1979).
- [36] A. Grisel and P. Schmid, *Polytypism and Lattice Vibrations of PbI<sub>2</sub>*, *Phys. Status Solidi B* **73**, 587 (1976).
- [37] N. Preda, L. Mihut, M. Baibarac, I. Baltog, and S. Lefrant, *A Distinctive Signature in the Raman and Photoluminescence Spectra of Intercalated PbI<sub>2</sub>*, *J. Phys. Condens. Matter* **18**, 8899 (2006).
- [38] H. Liu, Q. Chen, H.-S. Kim, N.-G. Park, and Y. Zhang, in *IEEE Photovoltaic Specialist Conference (PVSC)* (IEEE, New York, 2015).
- [39] J.-H. Im, H.-S. Kim, and N.-G. Park, *Morphology-Photovoltaic Property Correlation in Perovskite Solar Cells: One-Step versus Two-Step Deposition of CH<sub>3</sub>NH<sub>3</sub>PbI<sub>3</sub>*, *APL Mater.* **2** (2014).
- [40] Y. Zhao, A. M. Nardes, and K. Zhu, *Solid-State Mesoscaled Perovskite CH<sub>3</sub>NH<sub>3</sub>PbI<sub>3</sub> Solar Cells: Charge Transport, Recombination, and Diffusion Length*, *J. Phys. Chem. Lett.* **5**, 490 (2014).
- [41] V. D’Innocenzo, G. Grancini, M. J. P. Alcocer, A. R. S. Kandada, S. D. Stranks, M. M. Lee, G. Lanzani, H. J. Snaith, and A. Petrozza, *Excitons versus Free Charges in Organo-Lead Tri-Halide Perovskites*, *Nat. Commun.* **5**, 3586 (2014).
- [42] A. M. Soufiani, F. Huang, P. Reece, R. Sheng, A. Ho-Baillie, and M. A. Green, *Polaronic Exciton Binding Energy in Iodide and Bromide Organic-Inorganic Lead Halide Perovskites*, *Appl. Phys. Lett.* **107**, 231902 (2015).
- [43] I. Baltog, M. Baibarac, and S. Lefrant, *Quantum Well Effect in Bulk PbI<sub>2</sub> Crystals Revealed by the Anisotropy of Photoluminescence and Raman Spectra*, *J. Phys. Condens. Matter* **21**, 025507 (2009).
- [44] H. B. Bebb and E. W. Williams, in *Transport and Optical Phenomena*, edited by R. K. Willardson and A. C. Beer (Academic Press, New York, 1972), p. 239.
- [45] Z. Yong, B. Fluegel, M. C. Hanna, J. F. Geisz, L. W. Wang, and A. Mascarenhas, *Effects of Heavy Nitrogen Doping in III-V Semiconductors—How Well Does the Conventional Wisdom Hold for the Dilute Nitrogen “III-V-N alloys”?*, *Phys. Status Solidi C* **240**, 396 (2003).
- [46] T. Ohsaka, F. Izumi, and Y. Fujiki, *Raman Spectrum of Anatase, TiO<sub>2</sub>*, *J. Raman Spectrosc.* **7**, 321 (1978).
- [47] W. F. Zhang, Y. L. He, M. S. Zhang, Z. Yin, and Q. Chen, *Raman Scattering Study on Anatase TiO<sub>2</sub> Nanocrystals*, *J. Phys. D* **33**, 912 (2000).